

THE HONG KONG POLYTECHNIC UNIVERSITY

Full-Time BEng Honours Degree in Mechanical Engineering

Development of an Aerial Air Quality Monitoring Platform Based on Vertical Takeoff and
Landing (VTOL) Unmanned Aerial Vehicle (UAV)

by

Cheung Hiu Ching, Athena

Fung Ka Chun, Tim

Liu Sum Yin, Kylie

Report submitted in partial fulfilment of the requirements for the Honours Degree of
Bachelor of Engineering in Mechanical Engineering

19/04/2022

Acknowledgements

We would like to express our sincere gratitude and appreciation to the following supervisor, teachers, instructors, and teaching assistants who guided us to solve different problems in this final year project under the current COVID-19 pandemic. Their kindness and support helped us to get fruitful results in this project.

Prof. Chih-Yung WEN, Head and Chair Professor of Aeronautical Engineering, for his valuable advice and wholehearted support and supervision during this project.

Mr. Jeremy CHANG, Mr. Li-yu LO, Mr. Bailun JIANG, and Mr. Yurong FENG, for their professional techniques of UAV building and control and their kind comments.

Dr. Mei-po HO, Miss Kwok-ting Wong, Mr. Man-kit PANG, Mr. Kin FUNG, and Mr. Pak-wo SHUM for their all-round support in the manufacturing and mode designing of composited wings.

Mr. Zongnan CHEN, Mr. Zhengtong LI, Dr. Jiaao HAO, Ir. Wai Fong TANG, Ms. Qianyu ZHOU, and Mr. Jianhui FAN, for their useful guidance on CFD simulations and analysis.

Mr. Cheuk-kin CHEUNG, for his generous assistance on 3D scanning.

Summary of Contribution

Commented [CHCA[1]: All of us nd to write one]

Project: Development of an Aerial Air Quality Monitoring Platform Based on Vertical Takeoff and Landing (VTOL) Unmanned Aerial Vehicle (UAV)

Name of Student: H. C. Cheung

Names of group-mate(s): K. C. Fung and S. Y. Liu

This project involves the following tasks: (a) building VTOL Skywalker X8 UAV; (b) doing the flight test of the VTOL UAV without payload in Yuen Long; (c) doing the flight test analysis of the VTOL UAV; (d) doing 3D CAD drawing of composited wings based on some research data; (e) doing CFD simulation of the Clark Y airfoil and the airfoil of the Skywalker X8; (f) confirming the CAD drawing design of the composited wings; (g) designing the mold of the composited wing; (h) manufacturing the components of the composited wing in Industrial Centre; (i) writing the report.

We discussed all parts in this project. We also worked together in part (a), (b), (c), (f), (h) and (i) and I concentrated on part (a), (b), (d), (e), (g), and (h). I was mainly responsible for coordinating the tasks with my groupmates. I also did the final checking of the content of this report.

I chiefly wrote the section 1.1 - 1.2, 2.3 - 2.4, 3.1, 3.3 - 3.4, 4.1 - 4.2, 4.4 - 4.5, 4.6.1 - 4.6.3, 5.1 – 5.3, 6, and the appendix I to VI.

Summary of Contribution

Commented [CHCA[2]: All of us nd to write one

Project: Development of an Aerial Air Quality Monitoring Platform Based on Vertical Takeoff and Landing (VTOL) Unmanned Aerial Vehicle (UAV)

Name of Student: K. C. Fung

Names of group-mate(s): H. C. Cheung and S. Y. Liu

This project involves the following tasks: (a) building VTOL Skywalker X8 UAV; (b) doing the flight test of the VTOL UAV without payload in Yuen Long; (c) doing the flight test analysis of the VTOL UAV; (d) doing 3D CAD drawing of composited wings based on some research data; (e) doing CFD simulation of the Clark Y airfoil and the airfoil of the Skywalker X8; (f) confirming the CAD drawing design of the composited wings; (g) designing the mold of the composited wing; (h) manufacturing the components of the composited wing in Industrial Centre; (i) writing the report.

We worked together on literature reviewing and I focused on the comparison between different UAVs, material selection and the manufacturing of the composite wings as contained in section 2.3 and 2.5 respectively.

I was mainly responsible for (a), (e) and (h) in project tasks and meanwhile assisted in the other parts as well. For the report writing, the content was generally distributed according to the main works done by each groupmate so I have written the parts related to the composite material and the respective manufacturing processes in this report in chapter 4, 5 and 6.

Summary of Contribution

Commented [CHCA[3]: All of us nd to write one]

Project: Development of an Aerial Air Quality Monitoring Platform Based on Vertical Takeoff and Landing (VTOL) Unmanned Aerial Vehicle (UAV)

Name of Student: S. Y. Liu

Names of group-mate(s): H. C. Cheung and K. C. Fung

This project involves the following tasks: (a) building VTOL Skywalker X8 UAV; (b) doing the flight test of the VTOL UAV without payload in Yuen Long; (c) doing the flight test analysis of the VTOL UAV; (d) doing 3D CAD drawing of composited wings based on some research data; (e) doing CFD simulation of the Clark Y airfoil and the airfoil of the Skywalker X8; (f) confirming the CAD drawing design of the composited wings; (g) designing the mold of the composited wing; (h) manufacturing the components of the composited wing in Industrial Centre; (i) writing the report.

We basically discussed and worked together on all parts and I mainly concentrated on the part of the section of 3D scanning of the Skywalker X8, and also identify the definition of VTOL and UAV. In addition, I also concentrated in (a), (b), (d), (h). I was also responsible for the typesetting of the report.

For the report writing, the content that was generally distributed according to the main work done by each groupmate. Therefore, I mainly focus on the section mentioned above and also the Gantt chart for the actual progress.

Content

ABSTRACT.....	10
NOMENCLATURE.....	11
1. CHAPTER 1: INTRODUCTION.....	12
1.1. BACKGROUND	12
1.1.1. Air pollution monitoring in the Great Bay Area by a VTOL UAV.....	12
1.1.2. Airframe selection of the VTOL UAV.....	12
1.1.3. Reinforcement of the mechanical structure of a VTOL UAV	13
1.2. PREDICTABLE ISSUES AND PROBLEMS.....	14
1.2.1. During the design of a VTOL UAV.....	14
1.2.2. During simulation in Computational fluid dynamics (CFD)	14
1.2.3. During the composites manufacturing process.....	15
1.3. OBJECTIVES.....	15
1.4. MAJOR WORK OUTLINE.....	17
2. CHAPTER 2: LITERATURE REVIEW	18
2.1. INTRODUCTION OF UAV.....	18
2.2. INTRODUCTION OF VTOL.....	18
2.3. COMPARISON BETWEEN DIFFERENT TYPES OF UAV	18
2.3.1. Duration and range.....	19
2.3.2. Speed.....	20
2.3.3. Abilities	21
2.3.4. Conclusion of the UAV's comparison	22
2.4. AERODYNAMICS OF FIXED-WING VTOL UAV	23
2.4.1. During take-off and landing.....	24
2.4.2. During transitions	25
2.4.3. During cruise	26
2.5. COMPOSITE WING MANUFACTURING.....	26
2.5.1. Carbon fiber composites.....	26

2.5.2.	<i>Vacuum infusion</i>	28
2.5.3.	<i>Wet layup</i>	29
3.	CHAPTER 3: PROJECT PLANNING	31
3.1.	ORIGINAL PROJECT SCHEDULE.....	31
3.2.	GANTT CHART OF ACTUAL PROGRESS	32
3.3.	SUMMARY OF WORKS THAT HAVE BEEN FINISHED AFTER INTERIM REPORT	33
3.4.	INCOMPLETE GOALS	36
4.	CHAPTER 4: METHODOLOGY.....	39
4.1.	FLOWCHARTS OVERVIEW	39
4.1.1.	<i>Flowchart of building a VTOL UAV</i>	39
4.1.2.	<i>Flowchart of structure reinforcement by manufacturing composites wings</i>	40
4.1.3.	<i>Flowchart of vacuum infusion</i>	41
4.1.4.	<i>Flowchart of wet layup with vacuum bagging</i>	42
4.2.	VTOL SKYWALKER X8 UAV DESIGN.....	43
4.2.1.	<i>Specification of Skywalker X8</i>	43
4.2.2.	<i>Structure of Skywalker X8</i>	43
4.2.3.	<i>Take-off weight estimation</i>	44
4.2.4.	<i>Motor selection for VTOL part</i>	44
4.2.5.	<i>Required accessories</i>	46
4.2.6.	<i>Assembly of VTOL Skywalker X8</i>	47
4.2.7.	<i>Electronics of VTOL Skywalker X8</i>	48
4.2.8.	<i>Indoor flight test and preflight checking</i>	50
4.3.	3D SCANNING OF SKYWALKER X8	51
4.3.1.	<i>Scanning by using Vxelements</i>	52
4.3.2.	<i>Editing scanned files and merging results</i>	52
4.3.4.	<i>Converting entities from the cross-sections and building the 3D CAD files</i>	54
4.4.	REASONS OF SELECTING CLARK Y AIRFOIL	55
4.4.1.	<i>Better aerodynamics performance</i>	55

4.4.2.	<i>Flat lower surface and smoother upper surface</i>	56
4.5.	CALCULATION AND 2D SIMULATION IN CFD (AIRFOILS).....	57
4.5.1.	<i>Geometry setting</i>	58
4.5.3.	<i>Model selection in Ansys Fluent</i>	61
4.5.4.	<i>Calculation of length of first element of the edge in mesh</i>	62
4.5.5.	<i>Results of the dimensionless wall distances, $y +$</i>	64
4.5.6.	<i>Boundary conditions in Ansys Fluent</i>	65
4.5.7.	<i>2D airfoil simulation</i>	70
4.5.8.	<i>Convergence test</i>	72
4.5.9.	<i>Grid independence test</i>	72
4.6.	MANUFACTURING OF THE COMPOSITED WINGS.....	75
4.6.1.	<i>Composited wings design</i>	75
4.6.2.	<i>Mold design for the composited wings</i>	77
4.6.3.	<i>Connection of winglet and wing design</i>	80
4.6.4.	<i>Manufacturing process</i>	81
5.	CHAPTER 5: EXPERIMENTAL RESULTS AND DISCUSSIONS	89
5.1.	FLIGHT LOG ANALYSIS OF THE FLIGHT TEST OF VTOL SKYWALKER X8 UAV	
	WITHOUT PAYLOAD	89
5.1.1.	<i>Total hovering time during flight test</i>	89
5.1.2.	<i>Total cruising time during flight test</i>	90
5.1.3.	<i>General flight performance of VTOL Skywalker X8 UAV</i>	91
5.2.	SIMULATION RESULTS IN CFD.....	92
5.2.1.	<i>Comparison of the simulation and the Xfoil prediction of Clark Y airfoil</i>	94
5.2.2.	<i>2D simulation results of the airfoils</i>	96
5.2.3.	<i>Application of lifting line theory with the 2D simulation results</i>	99
5.3.	MANUFACTURING OF THE COMPONENTS OF COMPOSITED WING	108
5.3.1.	<i>Appearance of components of composited wing</i>	108
5.3.2.	<i>Dimensions of components of composited wing</i>	110

5.3.3. <i>Weight of components of composited wing</i>	112
6. CHAPTER 6: RECOMMENDATIONS FOR FUTURE WORK.....	114
6.1. FLIGHT TEST OF VTOL SKYWALKER X8 UAV WITH PAYLOAD	114
6.2. 3D CFD SIMULATIONS OF THE WINGS AND THE WHOLE VTOL UAV.....	114
6.3. WIND TUNNEL TEST FOR THE LIFT AND DRAG FORCES MEASUREMENT OF THE VTOL UAV	114
6.4. MANUFACTURING TWO COMPOSITED WINGS COMPLETELY.....	115
6.5. FLIGHT TEST OF VTOL UAV WITH COMPOSITED WINGS	115
7. CHAPTER 7: CONCLUSION.....	116
REFERENCES.....	117
APPENDIX I: VIDEO OF INDOOR HOVERING TEST	119
APPENDIX II: VIDEO OF FLIGHT TEST WITHOUT PAYLOAD	120
APPENDIX III: VIDEO OF VACUUM INFUSION FOR MANUFACTURING COMPOSITED WING.....	121
APPENDIX IV: COORDINATES OF CLARK Y AIRFOIL (CHORD LENGTH = 1 M).....	122
APPENDIX V: COORDINATES OF CLARK Y AIRFOIL (CHORD LENGTH = 382 MM).....	123
APPENDIX VI: COORDINATES OF SKYWALKER X8'S AIRFOIL (CHORD LENGTH = 382 MM).....	124
APPENDIX VII: LIST OF FIGURES.....	125
APPENDIX VIII: LIST OF TABLES.....	130

Abstract

A Vertical take-off and landing (VTOL) unmanned aerial vehicle (UAV) has the hybrid characteristics of a multi-rotor and a fixed-wing UAV which allow it to obtain distinctive performance in both duration, speed, and maneuverability among the other types. Therefore, it is suggested to be used for air quality monitoring in the Greater Bay Area. To achieve the specific needs of the task, this project would develop a new design of the VTOL UAV with the concern of capacity, strength, and aerodynamics.

First of all, an existing airframe would be selected and built with a designed VTOL part to test its characteristics. Then, after comparison between the choices in strength and density from the laboratory sources, alternative material, carbon fiber would replace the original material of the wings. The relative manufacturing process was also discussed and implemented. Furthermore, the wing was optimized by replacing the airfoil which can possess better drag and lift performance. The advanced aerodynamic performance would be also quantized by Computational Fluid Dynamics (CFD) simulation.

In this project, carbon fiber was selected as the new material for the wing due to its high strength and low density. Meanwhile, Clark Y airfoil was selected to replace the one in the original UAV frame. It was discovered that this type of airfoil can obtain a better performance and was more suitable for all stages of flying motion when the frame was customized from fixed-wing UAV to VTOL UAV.

Keywords: VTOL UAV; CFD; Carbon fiber wings

Nomenclature

α	Angle of attack (AOA)	m_4	Rear-left motor thrust	S	Wing area
δ_a	Angular deflection of ailerons	x_b	Front body axis	u	UAV velocity about x_b axis
δ_e	Angular deflection of elevator	y_b	Right body axis	v	UAV velocity about y_b axis
δ_r	Angular deflection of rudder	z_b	Down body axis	w	UAV velocity about z_b axis
δ_{thr}	Forward thrust force	γ_{mot}	p-factor rolling moment coefficient of motor thrust force	l	UAV moment along x_b axis
L_Q	Arm length for the quadrotor square of UAV	V_a	Magnitude of wind velocity relative to the UAV	m	UAV moment along y_b axis
c	Chord length	x	North position of UAV	n	UAV moment along z_b axis
C_L	Coefficient of lift (wing)	y	East position of UAV	p	UAV angular velocity about x_b axis
C_D	Coefficient of drag (wing)	z	Down position of UAV	q	UAV angular velocity about y_b axis
C_M	Coefficient of moment	u_P	“Plane” control vector	r	UAV angular velocity about z_b axis
ρ	Density of air	u_Q	“Quad” control vector	c_l	Coefficient of lift (airfoil)
y^+	Dimensionless wall distance	ϕ	Roll angle	c_d	Coefficient of drag (airfoil)
m_1	Front-right motor thrust	θ	Pitch angle	n	No. of divisions of edge sizing
m_2	Rear-right motor thrust	ψ	Yaw angle	U_∞	Freestream velocity
m_3	Front-left motor thrust	X	Vehicle state vector	φ	Arbitrary values of lifting line theory

1. Chapter 1: Introduction

1.1. Background

1.1.1. Air pollution monitoring in the Great Bay Area by a VTOL UAV

The air quality of the Greater Bay Area can affect millions of people's health. It is important to regulate air quality for the public health concern. Referring to the Innovation and Technology Fund (ITF) project, "Trial: Development of vertical take-off and landing (VTOL) unmanned aerial vehicle (UAV) for air quality monitoring in Greater Bay Area"[1], a traditional method is to send a quadrotor aircraft from a boat at a fixed location to detect the air quality of a limited area alongside the Pearl River. However, this method is time consuming and labor-intensive. Hence, from the ITF project[1], an air quality sensor, which is provided by the Hong Kong Environment Protection Department, aims to be carried by a VTOL UAV to conduct air quality monitoring of the Pearl River Delta Metropolitan Region (PRD).

1.1.2. Airframe selection of the VTOL UAV

Using a fast and long-range VTOL UAV can significantly increase the covered area of each flight. Thus, the efficiency of the monitoring can be greatly improved. Due to the heavy air quality sensor (around 1 kg) and its large size (191mm*79mm*71mm), we would like to choose an airframe with a large fuselage for carrying this bulky payload. Therefore, a swept wing aircraft, Skywalker X8 is chosen. In addition, the quadrotor part is installed at the Skywalker X8 for its VTOL function.



Figure 1.1 Our VTOL Skywalker X8 UAV

Figure 1.2 Dummy air quality sensor

1.1.3. Reinforcement of the mechanical structure of a VTOL UAV

Since the airframe of the Skywalker X8 is made of polystyrene, we hope to improve its hardness and strength by using composite materials. Also, we would like to redesign the airfoil and remove the winglets because the original design is not suitable for manufacturing the composite wings. Due to its winglets, the difficulties of manufacturing the wings by sticking around four layers of carbon fiber (CF) clothes on a mold increase. Consequently, we would like to choose an airfoil with a flatter design to reduce the complicated steps of manufacturing the composite wings. Besides, assuming the wing-tips vortices can be neglected because of the slow airspeed of our VTOL UAV, we will not design any new winglets for our new wings.

1.2. Predictable issues and problems

1.2.1. During the design of a VTOL UAV

The mechanical structure and the electronics setup would be the predictable issues during the building of our VTOL UAV. Since we would like to design an additional VTOL part on the selected airframe, we should make sure the structural design and the electronic arrangement of our VTOL UAV could be assembled and perform well to finish missions that were stated in the ITF project [1]. Therefore, the VTOL UAV should be tested without a payload to check its mechanical structures and its sensors' performance.

1.2.2. During simulation in Computational fluid dynamics (CFD)

As we would like to simulate the aerodynamics performance of the wings in CFD, the setting of the mesh and simulation of the CFD software, Ansys Fluent should be the predictable issues or problems. We had to find out the suitable setting to generate the mesh for doing the simulation in Ansys Fluent, which should be the most challenging task for this part as the setting of the mesh will affect the simulation results evidently. After getting the simulation results, we should compare the results with the standard data or prove the aerodynamics performance of the wings in the theoretical method.

1.2.3. During the composites manufacturing process

For the reinforcement of the VTOL UAV, it was predicted that there may be some issues or problems with the mold design and manufacturing process. It was because the handwork of the manufacturing process may need to be done by several trial and error, which would be a time-consuming task. Thus, the mold design should be well prepared before the manufacturing process to save time for revising. Besides, the installation of the accessories of the VTOL UAV should be also concerned after finishing the manufacturing of the carbon fiber wings.

1.3. Objectives

The project aims to develop a VTOL UAV for air quality monitoring in Greater Bay Area. This project needs to examine the traditional VTOL aircraft design and the design of the airflow inlet and output of the air quality sensor. Composite materials manufacture technics including mold design, are necessary to enhance the frame of the VTOL UAV. Essential electrical cabling and power system architecture are also required to link the payload and the flight control system. Based on the requirements, the objectives are listed as follows:

i) *Complete the flight task with the requirements*

According to the ITF project[1], a VTOL UAV should fly at a speed of 15 to 20 m/s for over 30 minutes and over 30 kilometres with a flight altitude of 100 to 500 metres. The matching lift/drag ratio surpasses 5, and the hover efficiency is within 30 percent of the ideal power loading, and the effective load fraction is no less than 30 percent of the gross weight. In this project, we aimed to flight our VTOL UAV for around 1 hour.

ii) *Redesign the wings*

During the project, a more challenging demand is necessary. Although the original Skywalker X8 can already achieve our goals, we would like to enhance the design of the wings to gain better results and simplify its manufacturing process. The Skywalker X8 should accomplish higher flight performance than before after remodelling the design.

iii) *Manufacturing the composited wings*

To achieve the above requirements and implement the best performances, the good material of the VTOL UAV is essential. The material should be light and hard enough. Therefore, before the structure reinforcement manufacturing progress, a comparison between the materials is needed. We finally decide to build a composited VTOL UAV due to the high stiffness and lightweight of the carbon fibre.

1.4. Major work outline

To achieve our goals in this project, several tasks were planned. There were three main stages in our progress.

i) The planning stage

We studied the characteristics of VTOL UAVs, fixed-wing UAVs, and quadcopters. We also learnt some basic aerodynamics and CFD techniques.

ii) VTOL UAV design

We built our VTOL UAV by using “Skywalker X8” as the airframe. Several calculations were done for the VTOL Skywalker X8, such as motor selection, total weight estimation, dimensions of the VTOL part and so on. Also, the flight test of the VTOL Skywalker X8 without the payload (the air quality sensor) was finished after the submission of the interim report.

iii) Composited VTOL UAV design

After the comparisons of the airfoils, we designed a new pair of wings for our composited VTOL UAV. The dimensions of the wings were done by 3D CAD drawing. Moreover, we did the 2D airfoils analysis with the CFD’s results. Then, we finished the mold design of the composited wings by 3D printing. Next, the manufacturing process of the composited wings had been started in the Industrial Center of the Hong Kong Polytechnic University.

2. Chapter 2: Literature Review

2.1. Introduction of UAV

Remote-control planes and drones are examples of unmanned aerial vehicles (UAV).

From Hu and Lanzon[2], an UAV generally is a plane that flies without a human pilot, crew, or passengers. Unmanned aerial vehicles (UAVs) are part of an unmanned aircraft system (UAS), which also includes a ground-based controller and a communications system with the UAV. Referring to Cary and Coyne[3], UAV flight can be controlled remotely by a human operator, as in a remotely piloted aircraft (RPA), or with varying degrees of autonomy, such as autopilot help, up to fully autonomous aircraft with no human interaction.

2.2. Introduction of VTOL

VTOL is a common technology of UAV. According to Laskowitz[4], an aircraft which can hover, take off, and land vertically is known as a vertical take-off and landing (VTOL) aircraft. Fixed-wing aircraft, as well as helicopters and other aircraft with powered rotors, such as cyclogyros, cyclocopters, and tiltrotors, are all included in this categorization.

2.3. Comparison between different types of UAV

In this comparison, we only focus on the UAVs which can be controlled by a remote controller and the power source of them should be LiPo battery only.

2.3.1. Duration and range

The different structures of UAVs lead to different durations and ranges. Fixed-wing-multi-rotor hybrid UAV (FWR-Hybrid UAV) has both vertical rotors and wings. A study of FWR-Hybrid UAV[5] stated that since FWR-Hybrid UAV has two goals of motors for generating lift and thrust respectively, it has greater power distribution than quadrotor. Hence, it consumes less battery to fly longer and further. However, as it carried more motors, the electricity economy and duration are lower than a fixed-wing UAV which usually just carries one motor. Figure 2.1 also shows that the FWR-Hybrid UAV can fly longer than the multi-rotor UAV but slightly shorter than fixed-wing UAV with the same weight, where these results can be estimated by comparing the data of the flight time per kg of each type of UAV[6].



Figure 2.1 UAV weight and payload vs. flight time [6].

Commented [CHCA[4]: Plz simply add a short para. of drone abilities (referring to papers), a table (example in our signal group), a conclusion para. for explaining the table, and move it to literature review

2.3.2. Speed

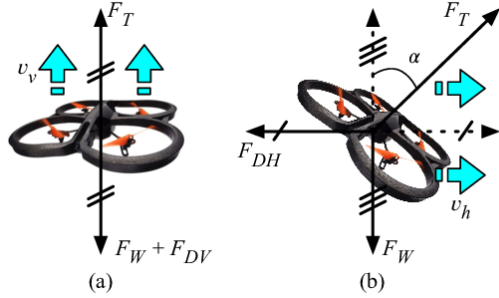


Figure 2.2 Forces on quadcopter in VTOL mode (a) and thrust mode (b) [7]

The speeds of different UAVs can be determined by analyzing their applied forces. For a quadcopter, it has to lean for moving forward because it has only four vertical rotors. In this situation, as explained through the force analysis with the free body diagram in Figure 2.2 [7], the thrust of the quadcopter is generated by sharing the lift force. Consequently, the speed of the quadcopter must always be slower than the fixed-wing UAV and FWR-Hybrid UAV the under same power out. Besides, as the fixed-wing UAV has the least aerodynamic drag, it is the fastest.

2.3.3. Abilities

To be versatile, an UAV should have high maneuverability. The existence of lift motors allows quadcopters and FWR-Hybrid UAVs to achieve more motions than fixed-wing UAVs. In the above comparison, FWR-Hybrid UAV has a higher speed and longer duration than a quadcopter. It turns out a result that FWR-Hybrid UAV can be applicable for more tasks. A study of FWR-Hybrid UAV[5] tested itself and a quadcopter to carry out air delivery and water sampling respectively. The results found that the FWR-Hybrid UAV performed better than the quadrotor, especially since the former one flies faster.

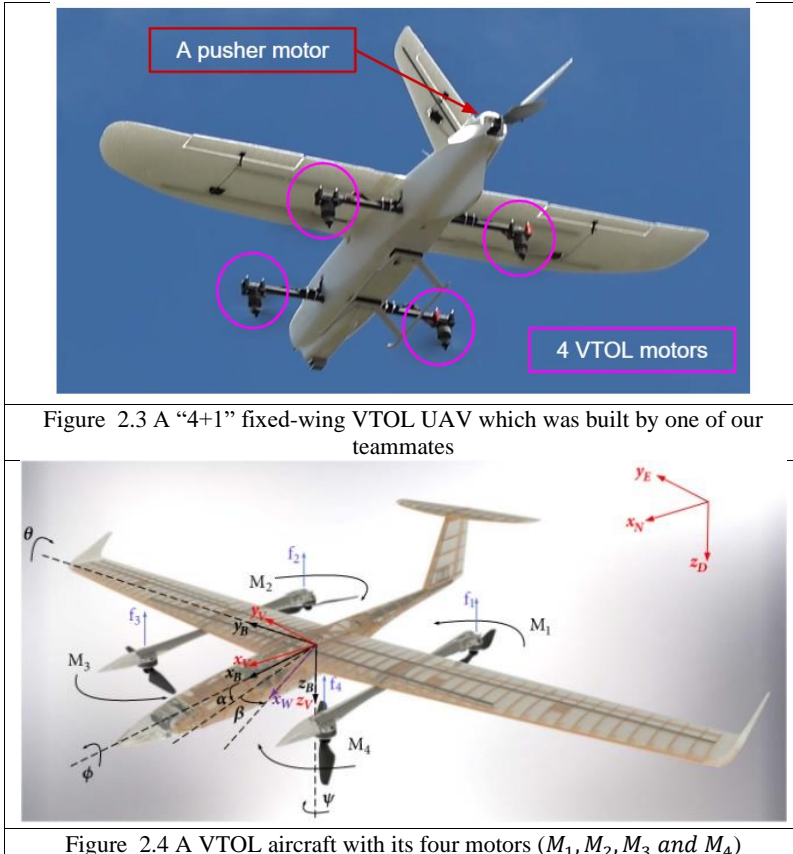
2.3.4. Conclusion of the UAV's comparison

According to the above analyses, FWR-Hybrid UAV combines the advantages of both fixed-wing UAV and quadrotor. It can obtain the high maneuverability of quadrotor and the high duration of the fixed-wing UAV.

	Fixed-Wing UAV	FWR-Hybrid UAV	Quadcopter
			
Flying Mechanism	Take-off and Landing, and Flying: A pair of wings & a pusher rotor	Take-off and Landing: Four rotors besides the fuselage Flying: A pair of wings, a pusher rotor & VTOL part	Take-off and Landing, and Flying: Four rotors as VTOL part
Shape	Streamlined shape	Hybrid of drone and fixed-wing UAV	X shape or Plus shape
Type(s) of motors	DC brushless motors & servo motors	DC brushless motors & servo motors	DC brushless motors
Duration	Very High	High	Low
Speed	Very High	High	Low
Maneuverability	Low	High	Very High

Table 2.1 Comparison of the UAVs

2.4. Aerodynamics of fixed-wing VTOL UAV



A full flight of a fixed-wing VTOL UAV includes its take-off, transition to cruise and landing, and landing. In this project, we would like to focus on “4 + 1” fixed-wing VTOL UAV which has four VTOL motors and one pusher motor. An example is shown in Figure 2.3. According to Mathur and Atkins[8], several equations can present the aerodynamics and dynamics of a fixed-wing VTOL UAV from its take-off to landing. Figure 2.4 indicates the axes and angles of a VTOL aircraft. The dynamic equation of the VTOL UAV during its whole flight is shown as follow:

$$\dot{X} = f(X, u_P, u_Q)$$

where $X = [x \ y \ z \ u \ v \ w \ \phi \ \theta \ \psi \ p \ q \ r]^T$, $u_P = [\delta_a \ \delta_e \ \delta_r \ \delta_{thr}]^T$,

$$u_Q = [m_1 \ m_2 \ m_3 \ m_4]^T$$

2.4.1. During take-off and landing

A fixed-wing VTOL UAV acts as a quadcopter with a pair of fixed-wing when it takes off and lands. Only the 4 VTOL motors will rotate while the pusher motor and all the elevons and ailerons will stop rotation. Hence, the aerodynamics of the VTOL UAV is similar to the one of the quadrotors. Therefore, the wing and tail aerodynamics forces and moments of the VTOL UAV are assumed to be negligible. Also, the airspeed of the VTOL UAV should be low for reducing the aerodynamics surface effects to support the above assumption. The forces and moments acting on the VTOL UAV during its vertical take-off and landing are:

$$\begin{bmatrix} F_x \\ F_y \\ F_z \end{bmatrix} = \begin{bmatrix} 0 \\ 0 \\ -(m_1 + m_2 + m_3 + m_4) \end{bmatrix} \text{ and}$$

$$\begin{bmatrix} l \\ m \\ n \end{bmatrix} = \begin{bmatrix} \frac{L_Q}{2} * (-m_1 - m_2 + m_3 + m_4) \\ \frac{L_Q}{2} * (m_1 - m_2 - m_3 + m_4) \\ \gamma_{mot} * (m_1 - m_2 + m_3 - m_4) \end{bmatrix}$$

where the p-factor, γ_{mot} should be found experimentally.

2.4.2. During transitions

There are two types of transitions of the fixed-wing VTOL UAV. From Mathur and Atkins[8], the Quad-to-Plane (Q2P) and Plane-to-Quad (P2Q) transitions must be executed for ensuring the VTOL performance and the forward propulsion system of the VTOL UAV can be function well.

For Q2P transition, it aims to provide a smooth transition from hover to the aircraft trim state for the cruise of the VTOL UAV. The velocities of the four VTOL motors will start decreasing while the pusher motor starts its rotation. The four VTOL motors will ramp down to zero when the rotation of the pusher motor remain steady. This can avoid the VTOL UAV suddenly dropping down due to zero thrust and give sufficient time for the VTOL UAV to reach its trim state. Hence, the VTOL UAV can do its cruise mission by its plane mode.

Conversely, for P2Q transition, a smooth transition from the aircraft trim state back to hover for landing should be provided. The tail rotor will start to ramp down and the elevator should pitch up in order to reduce the forward speed of the VTOL UAV. When the airspeed drops below enough, such as 1 m/s, the four VTOL motors can start the rotation and the VTOL UAV will act as a quadcopter to get ready for landing.

2.4.3. During cruise

Unlike during take-off and landing, the fixed-wing VTOL UAV acts as a plane rather than a quadcopter when it is cruising. The tail rotor will provide a forward thrust while some servo motors will control the movements of the ailerons, elevons and rudders. The aerodynamic lift, drag and moment of the VTOL UAV can be calculated at a given angle of attack, α for the wing from the relevant airfoil database with the aerodynamics coefficients.

$$Lift = \frac{1}{2} \rho V_a^2 S C_L; Drag = \frac{1}{2} \rho V_a^2 S C_D \text{ and } Moment = \frac{1}{2} \rho V_a^2 c S C_M$$

2.5. Composite wing manufacturing

2.5.1. Carbon fiber composites

Carbon fiber composites are now widely applied in many branches of industries for advanced purposes. They demonstrate high performance to the products by providing a high strength to weight ratio. From the findings of Material Science Research India[9], take the common intermediate modulus (type IM) of carbon fiber to compare, its modulus is between 200-350 GPa, which is close to that of steel (190-217 GPa) but at the same time its density ($1.76\text{-}1.93\text{g/cm}^3$) is much lower than those of steel ($7.75\text{-}8.05\text{ g/cm}^3$). Although the density of IM Carbon Fiber is higher than polystyrene which is the material of Skywalker X8's wings, it is still worth trading off for its strength. The total weight of the hollow carbon fiber wings can also be closer to the solid polystyrene one.

	IM Carbon Fiber	Steel	Polystyrene
Young Modulus	200-350 GPa	190-217 GPa	3-3.6 GPa
Density	1.76-1.93 g/cm ³	7.75-8.05 g/cm ³	0.96-1.05 g/cm ³

Table 2.2

Young modulus and densities of IM Carbon Fiber, Steel and Polystyrene[9]

While comparing with another popular composite-fiberglass, carbon fiber is still stiffer. Referring to the test by applying a pressure force of 500Pa at the bottom surface of the specific wing at center of pressure using ANSYS Static Structural[10], the total deformation of Epoxy-carbons is both smaller than the epoxy glass. It is also inspiring that carbon fiber composite can allow higher flexibility in airfoil design because of less concern on stiffness and weight.

Materials	Total deformation (mm)	Mode shape	Epoxy-Carbon UD	Epoxy S-Glass	Aluminum 2024 T3	Epoxy-Carbon Woven	Epoxy-E-Glass
Epoxy-carbon UD	4.223	1	0.84036	0.7176	0.60774	0.84665	0.7172
Epoxy S-glass UD	9.8794	2	1.38780	0.8117	0.61325	0.85416	0.7855
Aluminum 2024 T3	6.7377	3	1.10660	1.3689	0.60580	0.84461	1.3456
Epoxy-carbon Woven	7.9845	4	0.79319	0.7027	1.08580	1.50790	0.7043
Epoxy E-glass	10.943	5	1.63000	0.7843	0.62033	0.85557	0.7491
		6	1.61390	1.4494	0.63568	0.90700	1.4152

Figure 2.5
Wing deformation under pressure

Figure 2.6
Maximum amplitude(mm) of vibration of different materials and wing mode shapes[10]

Epoxy-Carbon UD and Epoxy-Carbon Woven are the two common carbon fiber composites. According to Figure 2.6, it can be seen that in most of the wing mode shapes, Epoxy-Carbon Woven has a lower maximum amplitude of vibration than that of Epoxy-Carbon UD and is close to the one of Aluminum 2024 T3. It implies that using this type of carbon fiber composite can help with the UAV's stability and thus less damage to the structure as well as the electronic parts inside.

2.5.2. Vacuum infusion

Vacuum infusion is one of the methods to fabricate carbon fiber reinforced polymer which is suitable for our CF wings. This method uses a vacuum pump to produce a pressure difference between two ends of the fiber. Therefore, the resin will be drawn into the fiber and the fiber can be hardened. This method requires lots of tools. There are two ends with one connecting the vacuum pump and the another connecting the resin pot. Each of the ends also links up the target fiber so that the resin can flow from the inlet to the outlet through the fiber. For the detailed and practical setup, it will be introduced in chapter 4.6.2.2.

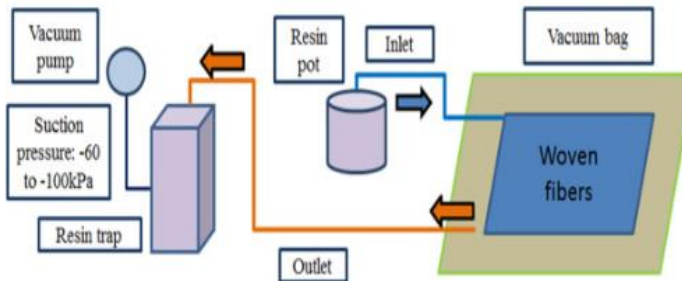


Figure 2.7 Working principle of vacuum infusion[11]

Referring to Hasim et al., since the infusion is conducted in a vacuum, the resin can be distributed evenly without excessive use of resin[11]. We can expect that the surface of our product is smooth, and the weight can be minimized due to the effective use of resin. However, it is also found that when the flow of resin decreases, the resin will accumulate at the center part of the fiber lay-up[11]. Therefore, the pressure in the vacuum bag must be controlled well and the bag must be sealed tightly.

2.5.3. Wet layup

Wet layup is another method to fabricate CF wing where the epoxy resin is directly smeared with a brush or sprayed on the carbon fiber fabric. This method is simple, and a comprehensive application of resin can be guaranteed. However, according to Calabresse et al. [12], it might be difficult to distribute the resin evenly. Thus, the drawbacks of the hand wet layup are uneven product surface and the addition of unnecessary weight due to the excess resin during the smearing [12]. **composted**

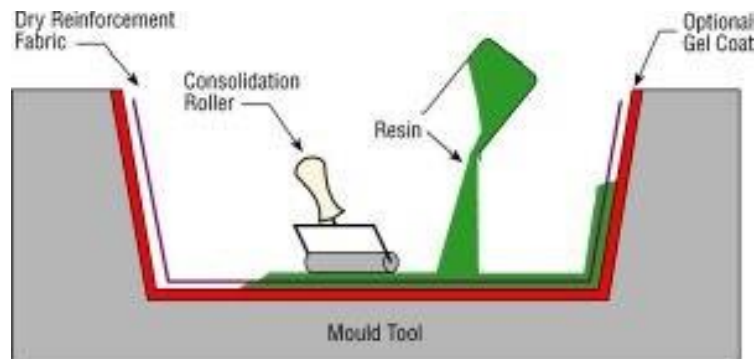


Figure 2.8 Wet hand layup method[13]

Therefore, following vacuum assisted molding is commonly applied. In the process, the carbon fiber mold smeared with the undried resin would be covered by absorbent fabric and placed into a vacuum bag. After that, there is vacuuming and high compaction under vacuum will flatten and absorb the excess resin on the surface. According to the research conducted by Shenoi and Dodkions, it was discovered that this method could cause high-quality fiber laminates and enhanced mechanical properties with improved uniformity. Due to the compaction on the product, air voids were also eliminated[14]. The following experiment of the research also found and stated that with this method 15% of the weight on single skin parts can be saved[14]. To manufacture high-quality products, this project would adopt the wet layup with vacuum assisted molding to manufacture the carbon fiber wings. The detailed process and setup will be introduced in chapter 4.6.2.3.



Figure 2.9 Wet layup method with vacuum assisted molding

3. Chapter 3: Project Planning

3.1. Original project schedule

Description	Start date	End date	Duration (days)
Planning	01/08/2021	22/08/2021	22
To understand the requirements of the flight mission	01/08/2021	01/08/2021	1
To understand differences between VTOL UAVs, fixed-wings UAVs & quadcopters	08/08/2021	22/08/2021	15
VTOL UAV Design	22/08/2021	31/12/2021	131
To do calculation of VTOL Skywalker X8 design	22/08/2021	22/09/2021	32
To build VTOL Skywalker X8	23/08/2021	05/11/2021	75
To test & do flight logs analysis of VTOL Skywalker X8 (without & with payload)	06/11/2021	31/12/2021	56
Interim report	01/09/2021	22/11/2021	83
Composited VTOL UAV Design	22/09/2021	12/04/2022	203
To do 3D CAD drawing of our composited VTOL UAV after doing research	22/09/2021	29/11/2021	69
To do 2D and 3D analysis with CFD's results of composited wings & VTOL UAV	30/11/2021	29/12/2021	30
To design the CF mold & manufacture the composited wings	15/12/2021	05/02/2022	53
To assembly composited wings and do the pre-flight test	06/02/2022	23/03/2022	46
To do fly test & data analysis with CFD's results of composited VTOL UAV	24/03/2022	12/04/2022	20
Final report	05/03/2022	19/04/2022	46

Table 3.1 Original project schedule

Commented [LS[5]: The original text is "08/01/2021", I think it should be a typo so I changed it. Just change it back if I'm wrong. Thanks.

Commented [CHCA[6R5]: Ya it's a typo, thxxxx

3.2. Gantt chart of actual progress

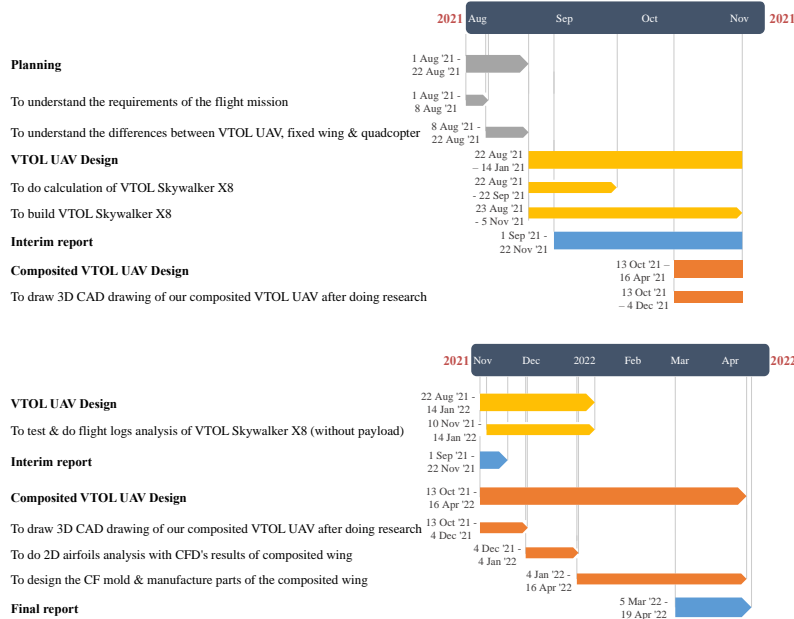


Figure 3.1 & 3.2 Gantt chart of actual progress under pandemic

3.3. Summary of works that have been finished after interim report

i) Fly test without payload

Before the submission of our interim report, we could only finish the indoor hovering test of our VTOL Skywalker X8. Thus, we finished the Fly test (without payload) of the VTOL Skywalker X8 in Yuen Long. During the test, we collected a set of flight data that was more comprehensive than the indoor test. Eventually, through the study of the data, it came up with the estimated time of hovering and cruising time and other general performances which are valuable for the future design of our own UAV. The analysis details would be mentioned in the following sections.



Figure 3.3 Flight test of Skywalker X8 without payload in Yuen Long

ii) CFD Simulation

In the interim report, according to the laboratory sources, we found that Clark Y was a more ideal airfoil for the mission stated in this project. In order to study more about the aerodynamic performance and prove our discovery, an airfoil CFD simulation had been done. The simulation generated the coefficients of lift and drag with different angles of attack of both airfoils. The results had shown that the overall performance of Clark Y was better than the original airfoil in Skywalker X8. The details of the simulation setting, and results would be presented in the following chapters.

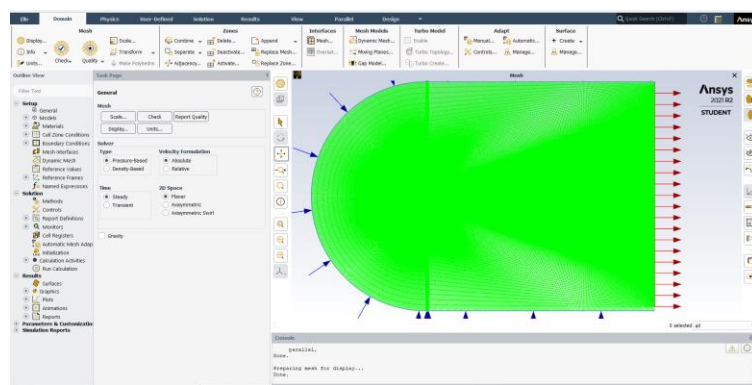


Figure 3.4 Simulation of Clark Y airfoil by Ansys Fluent

iii) Design composited wings with Clark Y airfoil and the mold

After finishing the airfoil simulation and the application of the lifting line theory, we used the Clark Y airfoil to design the composited wings with a 50 mm transition, which was for assembling with the original fuselage. The molds of the composited wings were designed according to the vacuum infusion and the wet layup methods. The design details would be shown in the following sections.

iv) Manufacturing 3 parts of composited wings

Since carbon fiber was chosen as the material for the new wings, different manufacturing processes were studied. Finally, with the concerns of product quality and the feasibility of the processes, vacuum infusion and wet layup were approached to manufacture three parts of a composite wing. For the details of the manufacturing processes and the quality of the products, they will be discussed in the following chapters.



Figure 3.5 Composite wing parts manufactured in this project (without mold

release)

3.4. Incomplete goals

Due to COVID-19, several signs of progress of our project have been affected. The tasks in red colors are the incomplete missions in Table 3.1. The details of how COVID-19 affect the progress are shown below.

i) 3D Simulation

One of the original plans for the CFD simulation was a 3D simulation. However, the results were not sensible that the lift of the model defined by the simulator is -11.58494. In general, the coefficient of the lift of an aircraft model which can fly successfully would not be negative. Eventually, we realized that it may be due to the limited number of cells of the student license of Ansys, we could not do the simulation for the objects that need to have a huge mesh size. Besides, we were not suggested to come to school so we could not use the computer in the laboratory to do the simulation. Because of the limited calculation load of our laptops, we could not do the simulations with a high number of iterations, which also affect the accuracy of the results.

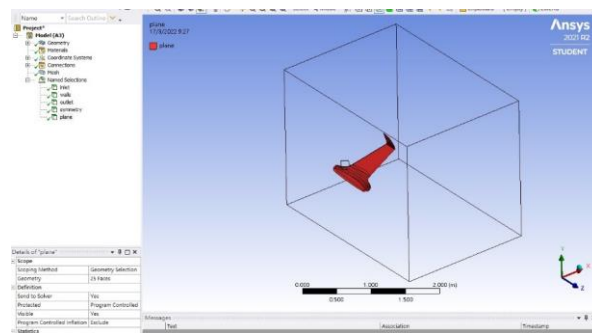


Figure 3.6 3D X8 model in Ansys Fluent

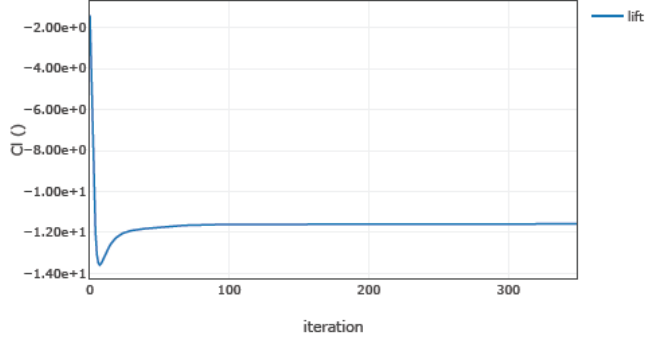


Figure 3.7 c_l graph of the 3D Skywalker X8

ii) Manufacture of Final Product

In this project, a final product should be made. However, the transportation of the 3D printing molds was influenced by COVID-19. In addition, since the Industrial Centre temporary suspended its services due to COVID-19, the components of the composited wings could not be manufactured on time too. Consequently, we could only order the molds of a wing and manufactured three components of the wing before the submission of this report.

Following the original planning, to consider the assembly of the composited wings and the VTOL part, they could be stuck together with resin matrices. It was because both of them were made of carbon fiber. Therefore, the wings did not require to be cut or drilled for inserting their connection parts of the carbon fiber tubes in the VTOL part. The mechanical structure of the composited wings could be less affected.

In addition, for the installation of the servo motors, there would be some 3D printing stands for holding each servo motor in the composited wings. A small hole would be drilled on the bottom of each wing for inserting the servo motors to control the elevons.

iii) Flight Test

Due to the government policies under COVID-19, the International Model Aviation Centre in Yuen Long did not open to the public according to the social distancing measures. Thus, only the flight test of the VTOL Skywalker X8 UAV without payload in December 2021 could be finished.

The original plan was to have two more flight tests. The first one should be the flight test of the VTOL UAV with the payload by using the same approach before. The second one is the trial to fly the composited VTOL UAV with the payload. The data collected during the flight will be used as a comparator to the other flight logs.

4. Chapter 4: Methodology

4.1. Flowcharts overview

4.1.1. Flowchart of building a VTOL UAV

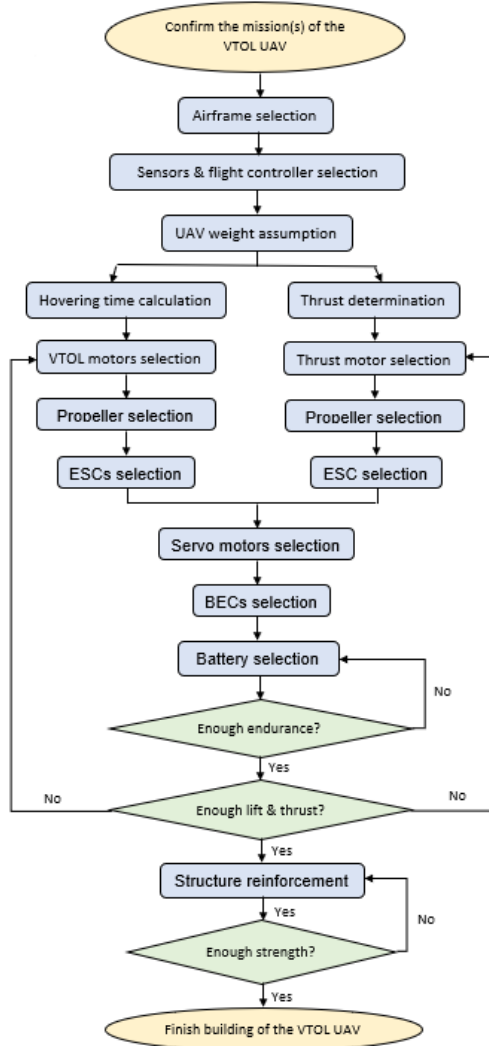


Figure 4.1 Design flowchart of building a VTOL UAV

4.1.2. Flowchart of structure reinforcement by manufacturing composites wings

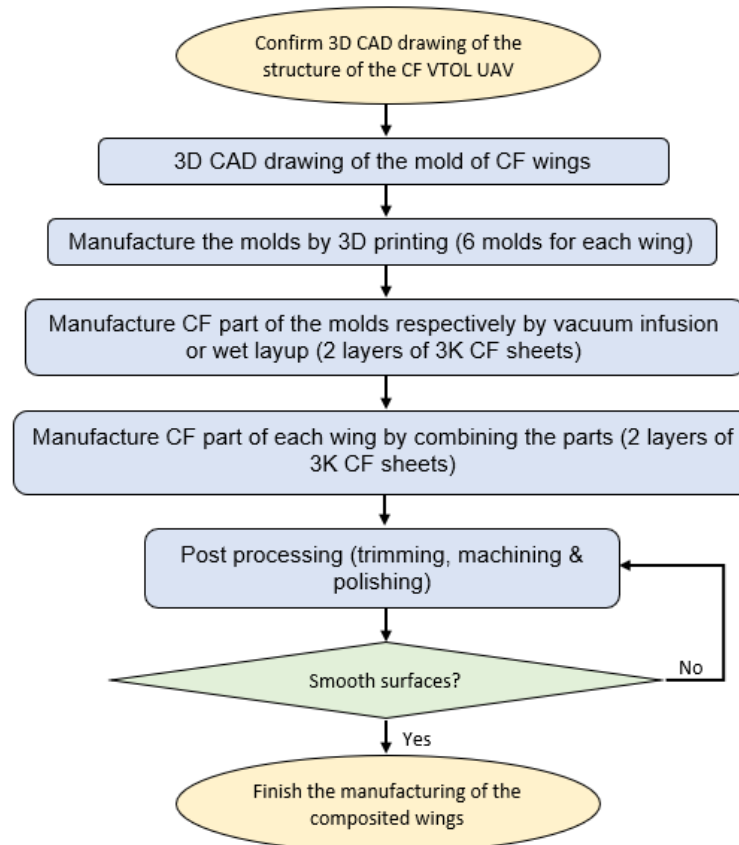


Figure 4.2 Design flowchart of manufacturing of composites wings

4.1.3. Flowchart of vacuum infusion

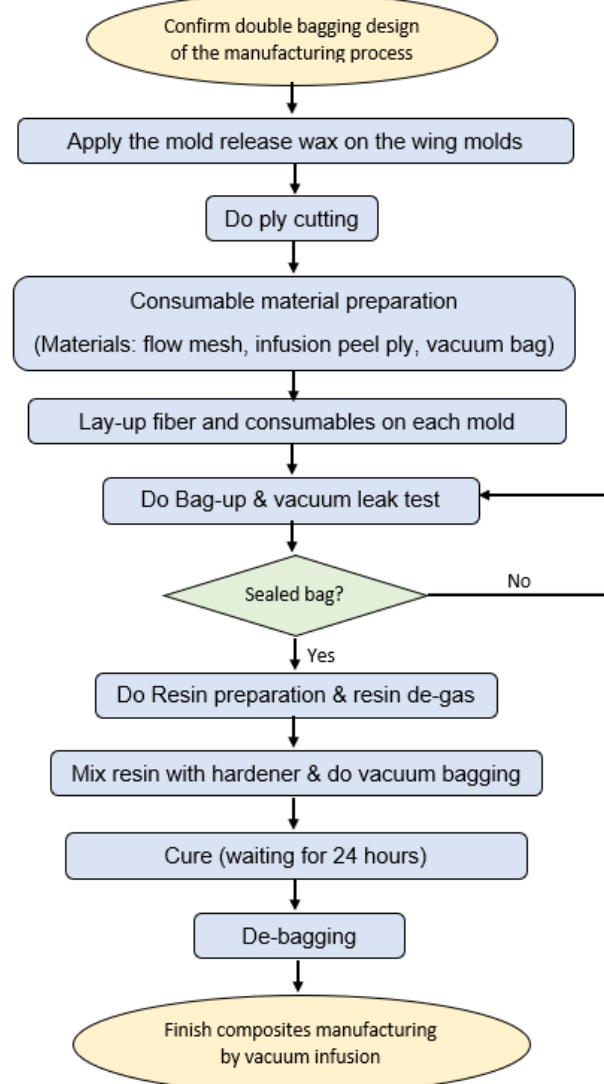


Figure 4.3 Design flowchart of vacuum infusion

4.1.4. Flowchart of wet layup with vacuum bagging

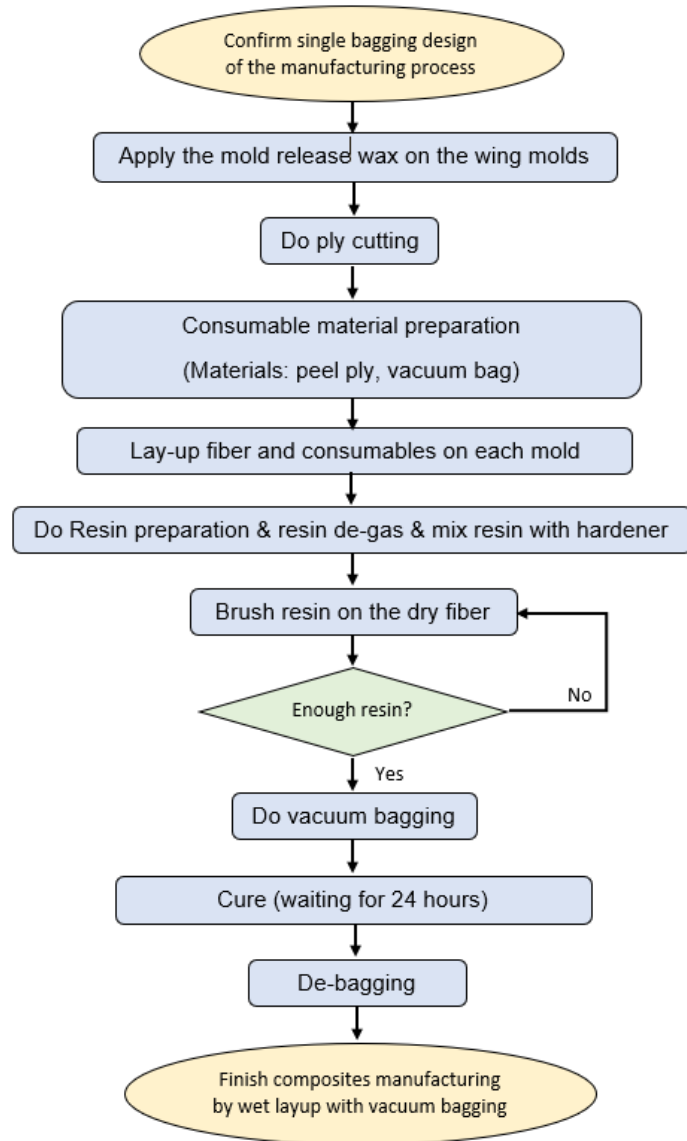


Figure 4.4 Design flowchart of wet layup with vacuum bagging

4.2. VTOL Skywalker X8 UAV design

4.2.1. Specification of Skywalker X8

Wingspan	2120 mm	Wing area	0.8 m^2
Fuselage length	790 mm	C.G.	From head to back 430-440 mm

Table 4.1 Specification of Skywalker X8[15]

4.2.2. Structure of Skywalker X8



Figure 4.5 Structure of Skywalker X8

The main structure of the Skywalker X8 can be divided into winglets, wings, and fuselage. There are also two orange plastic connectors which are the linkages between the fuselage and the wings. This design can provide a quick installation or disassembly of the wings so that we can transport the Skywalker X8 by separating its fuselage and wings. This increases its portability.

4.2.3. Take-off weight estimation

Item	Weight (g)	Quantity	Total weight (g)
Airframe: Skywalker X8 (Fuselage + wings)	1500	1	1500
Servo motor (EMAX ES3104) & BEC	19.5	2	39
Carbon fiber tube (length: 889mm)	37	1	37
Carbon fiber tube (length: 589mm)	24.9	1	24.9
Carbon fiber tube (length: (956mm)	135	2	270
ESC	20	5	100
Flight controller: Pixhawk 4	33.1	1	33.1
GPS & Gyroscope & Safety switch	35.1	1	35.1
Airspeed sensor (Holybro Digital Air Speed Sensor)	45.4	1	45.4
Radio Telemetry	20	1	20
2.4 GHz Receiver (FrSky TFR8 SB Receiver)	11.4	1	11.4
Wi-Fi Module	5	1	5
Payload (Dummy air quality sensor)	910	1	910
		Total weight (g)	3030.9

Table 4.2 Take-off Weight Estimation before VTOL motors selection

The weights of the basic electronics such as sensors and flight controllers are measured. The total weight of the Skywalker X8 excluded the VTOL part is assumed and shown in the above table.

4.2.4. Motor selection for VTOL part

The performances of all motor-propeller combination candidates are processed via the excel with thrust/current data collected from the manufacturers. The assume total weight includes the assumed take-off weight in Table 4, assumed weight of pusher motor, weight of the specific four motors and the four propellers. One example is shown as follow:

Assumed weight of accessories (g)	3030.9	Sunnysky X3120-III
Assumed weight of pusher motor (g)	159	
Motor	Propeller	Voltage (V)
Sunnysky V4014 (KV330)	EOLO/CN15*5.5	22.2
		Weight (g) (4 motors)
		664
		Weight (g) (4 propellers)
		84
	Thrust (g)	Current (A)
	0	0
	500	2
	750	3.3
	1000	4.9
	1250	6.8
	1500	8.8
	1750	11.05
	2073	14.1
Required equation: ax^2+bx+c		
a	b	c
2.00E-06	0.0032	-0.0406
Assume total weight (g)	3937.9	
Assume total current (A)	20.19	
Assumed Depth of discharge (DOD)	0.70	
Required energy capacity (mAh)	28846.29744	
Hovering time (min)	45.75977222	
Weight/Thrust (%)	47.49035215	

Sunnysky V4014 (KV330) 22.2V EOLO/CN15*5.5

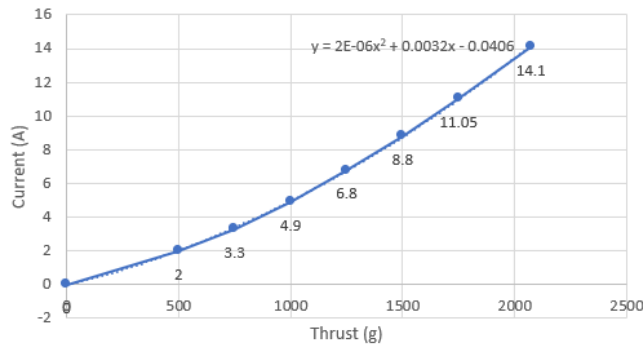


Figure 4.6 Motor-propeller performance analysis

And the comparison of the motor-propeller combinations is:

Motor	Propeller	Voltage (V)	Weight/Thrust (%)	Hovering time (min)
Sunnysky V4014 (KV330)	EOLO/CN15*5.5	22.2	47.49	45.76
Sunnysky V4014 (KV330)	EOLO/CN15*5.5	25	38.68	59.75
Sunnysky V4014 (KV330)	EOLO CN17*6.2	22.2	35.49	58.25
Sunnysky V4014 (KV330)	EOLO CN17*6.2	25	29.58	62.81
T-motor 4006 (KV380)	T-motor 13*4.4CF	24	53.87	60.55
T-motor 4006 (KV380)	T-motor 14*4.8CF	24	44.79	60.44
T-motor 4006 (KV380)	T-motor 15*5CF	24	40.03	64.56
Tarot 5008 (KV340)	Falcon 1855CF	22.2	34.20	47.33
T-motor MN4014 (KV330)	T-motor 15*5CF	22.2	40.71	52.74
T-motor MN5208 (KV340)	T-motor 15*5CF	24	38.22	49.26
T-motor MN5208 (KV340)	T-motor 16*5.4CF	24	39.41	49.16

Table 4.3 Comparison of different motor-propeller combinations

Regarding to the hovering time estimation, T-motor 4006 (KV380) with T-motor 15*5CF can provide longest hovering time, 64.56 minutes, so it is selected. Besides, it has an acceptable weight/thrust ratio which is below 50%.

4.2.5. Required accessories

Airframe	Skywalker X8
Flight Controller	Pixhawk 4 (Software: AutoPilot)
Power Management Board	Holybro Pixhawk 4 Power Module (PM07)
VTOL Motors	T-motor 4006 (KV380)
VTOL motors' Electronic Speed Controller (ESC)	HobbyWing XRotor 40A
Thrust Motor	Sunnysky X3120-III
Thrust motor's ESC	HobbyWing FlyFun V5 60A
Servo Motors	EMAX ES 3104
Servo Motors' Battery Eliminator Circuit (BEC)	HobbyWing UBEC 5V
VTOL propellers	T-motor 15*5CF (diameter*pitch)
Thrust motor propeller	13*8 (diameter*pitch)
GPS & Gyroscope & Safety Switch	HolyBro Pixhawk 4 Neo-M8N GPS
Airspeed sensor	Holybro Digital Air Speed Sensor
2.4 GHz Receiver	FrSky TFR8 SB Receiver
Power	Grignard Ace Tattoo LiPo Battery 22.2V

Table 4.4 Accessories of the VTOL Skywalker X8

4.2.6. Assembly of VTOL Skywalker X8

Since we would like to transform the Skywalker X8 to a VTOL UAV, it is necessary to construct the stands for mounting the four rotors. The solution is to add two carbon rods below the wings with a mount on each. Figure 4.7 presents the mounts of the VTOL part below.



Figure 4.7 Overview of the VTOL part of our VTOL Skywalker X8 UAV



Figure 4.8
Electronics wires are inserted into the carbon fiber tubes

To install the four brushless motors as the VTOL motors on the Skywalker X8, two extra carbon tubes are added. As only two carbon rods and the orange plastic connectors above are the original supporting components for mounting the wings, we designed a mounting, which is made by 3D printing, to be the linkage of the carbon rods and the extra carbon tubes. The mounting is stuck under each polystyrene wing by expanded polystyrene glue. Several holes are drilled on the tubes for mounting the VTOL motors and fixing the position of the tubes with the 3D printing mounting. The electronics wires of the motors and their ESC are inserted into the tubes to prevent the broken wires connection due to any accidents during future flights.

4.2.7. Electronics of VTOL Skywalker X8

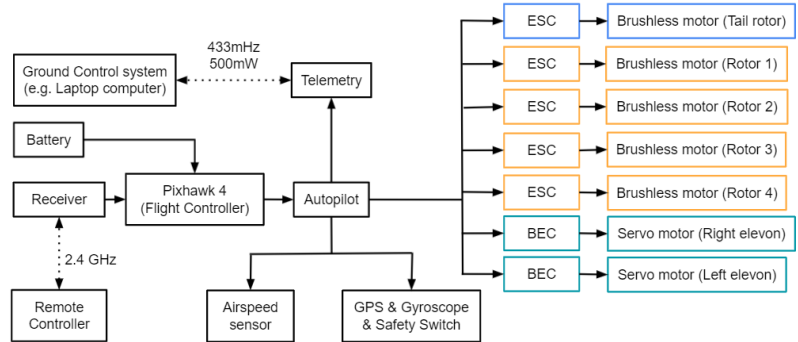


Figure 4.9 Connection of the VTOL Skywalker X8 UAV's electronics components

The main concept of the electronics arrangement in Figure 4.9 is to connect all the actuators and sensors to the flight controller (Pixelhawk 4) so that the controller can process the received signal and control the whole movement of the VTOL Skywalker X8 UAV. The servo motors are supported by the Battery Eliminator Circuit (BEC) while the brushless motors are supported by the electronic speed control (ESC). Apart from these, an airspeed sensor is connected to transfer the collected data back to the ground. Meanwhile, the GPS with gyroscope and safety switch can locate and guide the VTOL UAV by providing the positioning data during flight. A 2.4 GHz remote controller is used to control the VTOL UAV via a receiver. Those sensors and motors work properly under the control of the Pixelhawk 4 and its software suite (software: Mission Planner).

For achieving a better management of the external wires of the VTOL part, the wires which inserted into the carbon tube are grouped at each wing. Figure 4.10 shows the wires inside a wing. Thus, there are 2 connectors (XT60 and MT30) expose from each wing. At each wing, all the positive and ground wires of the actuators' ESC or BEC are connected by a XT60 connector, while all the signal wires of the actuators are connected by a MT30 connector. Both connectors link to a power management board in Figure 4. 11. This board can connect the battery and the actuators with Pixhawk 4 for managing the order of the wires and indicating the usage of the wires clearly. Therefore, even wires of the wings' actuators can be connected easily during the assembly by plugging only 4 connectors in total.

	
Figure 4.10 Electronic wires management inside a wing	Figure 4.11 Power Management board in VTOL Skywalker X8 UAV

4.2.8. Indoor flight test and preflight checking



Figure 4.12 Indoor hovering test of VTOL Skywalker X8

Before flying the VTOL Skywalker X8 in the outdoor flying field, an indoor hovering test should be induced to ensure the flight performance of the VTOL UAV is stable. The rotating direction of each actuator should be checked to ensure the performance of the VTOL UAV for safety concern. Moreover, the abilities of the sensors should be confirmed before flying the VTOL UAV too.

The hovering test of our VTOL UAV is shown in Figure 4.12.

4.3. 3D scanning of Skywalker X8

The CAD drawing of the Skywalker X8 was created by 3D scanning. The purposes of scanning the Skywalker X8 into a digital file are because some calculations and simulations of the Skywalker X8 are needed to enhance its VTOL design for better performances. Since the Skywalker X8 is quite large which cannot be 3D scanned automatically, we would like to use a portable optical measuring device, handySCAN to do the 3D scanning (Figure 4.13). After the 3D scanning, some aftereffects are required to clean up the noise of the scanned files of the object into a full 3D model. Then, some sketches are added to convert the cross-section entities. Finally, exports the CAD drawing to SolidWorks for building the 3D CAD drawing.

The details of the 3D scanning are listed in the following:

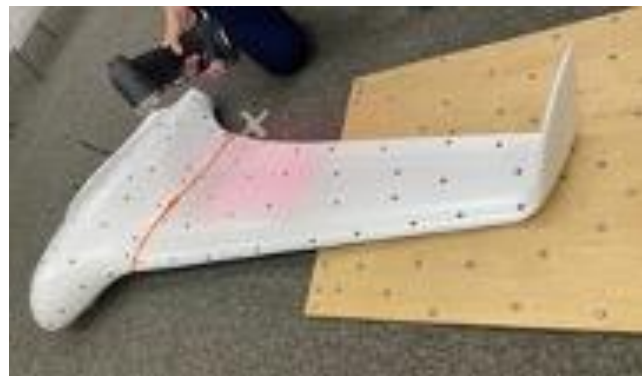


Figure 4.13 Using handySCAN to do the 3D scanning

4.3.1. Scanning by using Vxelements

A software named Vxelements is used to help scan the Skywalker X8. The handySCAN is a moveable scanner that can be moved around all the angles by using hands. The limitation is that some dot labels needed to be stuck on a plane or the Skywalker X8 to be the references point to outline the structures of the UAV. To complete a whole 3D structure of the UAV, different angles are needed to scan. The different scanning angles should be at least three points in triangle shape overlapping with other angles to be the references points for merging.

4.3.2. Editing scanned files and merging results

After scanning all the parts and angles, Geomagic Design X should be used to edit the scanned file and merge the different views into a 3D part. First, the scanned files usually got lots of noise. Those noise needed to be deleted and some of the erroneous drafts.

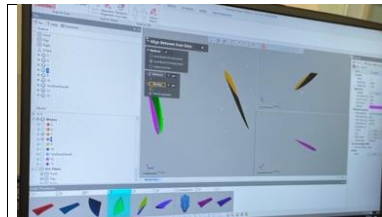


Figure 4.14
Progress while aligning the wing

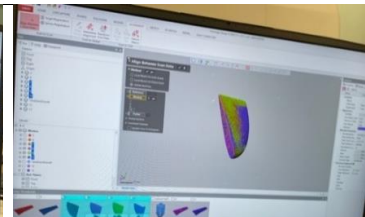
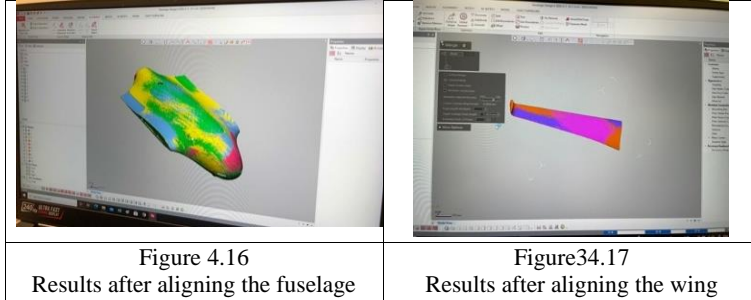


Figure 4.15
Results after aligning the wing



To merge different views of the parts into a 3D part, a function called align in Design X is needed. First, select the three points mentioned above, which help to be the references points. Both views should be selected with the same point. After aligning the different views, the results should be shown like in Figure 4.15. The colour should be evenly distributed. During scanning the Skywalker X8, at least four views of a part are being scanned. Figure 4.16 and Figure 4.17 show the results after aligning the fuselage and the wing. Both colours are evenly distributed. After aligning all the parts, ‘merge’ is needed to group all the views into parts.

4.3.4. Convening entities from the cross-sections and building the 3D CAD files

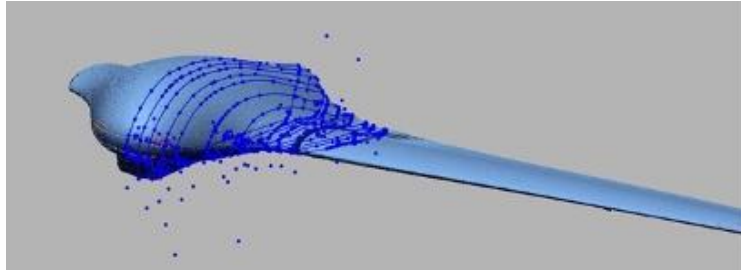


Figure 4.18 Convening the cross-section into entities

Some reference entities need to be converted before exporting the files to SolidWorks for further sketching. Several entities in Figure 4.18 have been transformed into references. Every 15 to 30 cm, a reference is placed. The noise in the entities should be removed after exporting them to SolidWorks, and the entities should be smoothed out. The entities converted in Design X are not smooth enough, and some noise may be converted, affecting the entity completeness. Figure 4.19 to Figure 4.21 show the results. The 3D parts can start building utilizing the loft surface after altering the entity designs and turning them solid. These represent in Figure 4.22 to Figure 4.24.

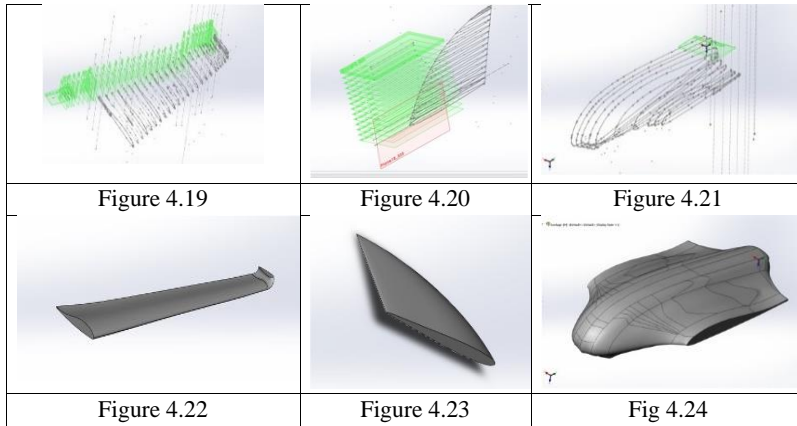
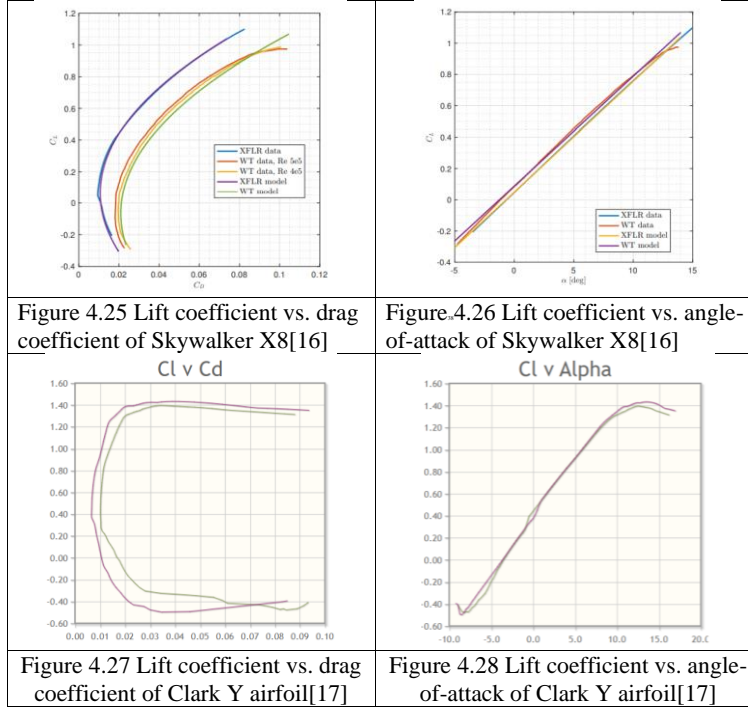


Figure 4.19 – 4.24 3D scanned curves and their CAD drawing

4.4. Reasons of selecting Clark Y airfoil

4.4.1. Better aerodynamics performance

In the aerodynamics aspect, we would like to choose an airfoil with higher c_l / c_d ratio and c_l / α ratio for assuring better flying performance of our composited VTOL UAV. Referring to Gryte et al.[16], the relevant graphs of the data are shown in Figure 4.25 to Figure 4.26. Regarding the data of Clark Y airfoil, the Airfoil Tools[17] indicated them in Figure 4.27 to Figure 4.28. Assume the aerodynamics performance of the Skywalker X8 can be similar to its airfoil. As Clark Y airfoil can have higher c_l/c_d ratio and c_l/α ratio than Skywalker X8's, we selected this airfoil for our composited VTOL UAV.



4.4.2. Flat lower surface and smoother upper surface

In the manufacturing aspect, the difficulty of demolding a composited curved surfaces part is much greater than the one of a composited flat surfaces part.

Figure 4.29 shows the shape of the Clark Y airfoil, which has a flatter lower surface and a smoother upper surface than the airfoil of the Skywalker X8.

Therefore, we would like to choose the Clark Y airfoil due to its better surfaces.

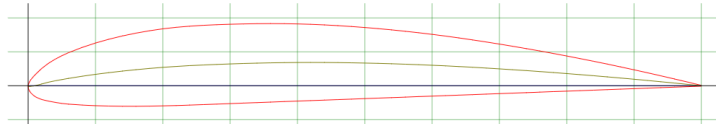


Figure 4.29 Shape of Clark Y airfoil[17]

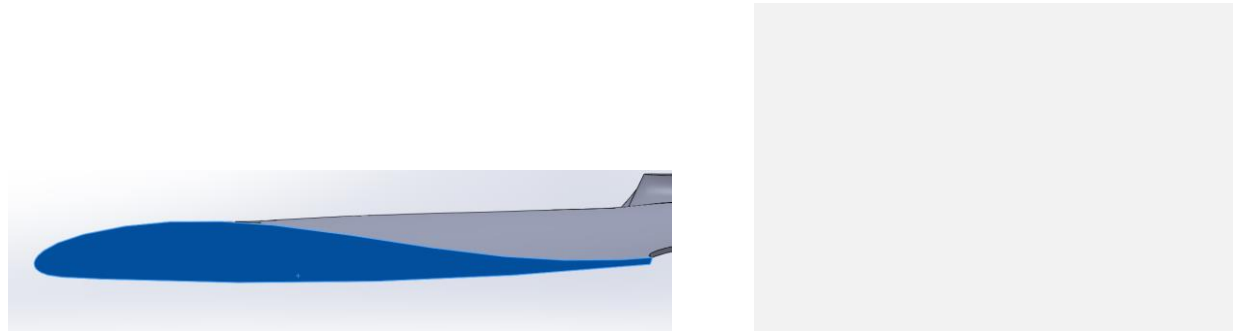


Figure 4.30 Shape of the airfoil of Skywalker X8

4.5. Calculation and 2D simulation in CFD (airfoils)

Ansys fluent is a common commercial CFD software. We had used this software to do the 2D simulation of the Clark Y airfoil with 1 m chord length, the Skywalker X8's airfoil with 382 mm chord length, and the Clark Y airfoil with 382 mm chord length. The two airfoils with 382 mm chord length referred to the size of the wings of our VTOL UAV, while the airfoils with 1 m chord length referred to the information of the standard data of Clark Y airfoil. We would like to compare the simulation results of the Clark Y airfoil with 1 m chord length to the Xfoil prediction of the Clark Y airfoil to ensure our setting in Ansys fluent was correct. Then, referring to the proved setting, we could compare the simulation results of the two airfoils with 382 mm chord length. This comparison could show whether the airfoil of our composited wings could have a better aerodynamics performance or not.

4.5.1. Geometry setting

Import coordinates of airfoils

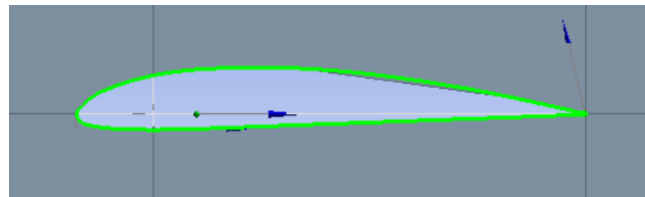


Figure 4.31 Imported Clark Y airfoil with chord length = 1 m

For the 2D airfoil simulation in Ansys Fluent, we should first import the x, y, and z coordinates of the airfoils. Since the airfoils are in 2 dimensions, the z coordinates must be 0. The .txt files of the coordinates of the three airfoils are shown in the Appendixes. Also, we found that the order of the coordinates should be started from the leading edge to the trailing edge. Otherwise, the software could not generate the curve if the first and the last y coordinates were not 0.

Dimension of wind tunnel

The shape of our wind tunnel was combining a semi-circle and a square. To prevent the blockage effect, we would like to calculate the minimum diameter or height of the wind tunnel.

$$\text{Blockage ratio} = \frac{\text{thickness of airfoil}}{\text{diameter or height of wind tunnel}}$$

Assume our largest acceptable blockage ratio is 5%. The thickness of the Clark Y airfoil with 1 m chord length \approx 12 cm = 0.12 m. Thus,

$$\text{Min. diameter or height of wind tunnel} = \frac{0.12}{0.05} = 2.4 \text{ m}$$

As we would like to use the proven setting of the Clark Y airfoil with 1 m chord length for the other two airfoils' simulations, we do not need to calculate the minimum diameter or height of the wind tunnel for the airfoils with 382 mm chord length.

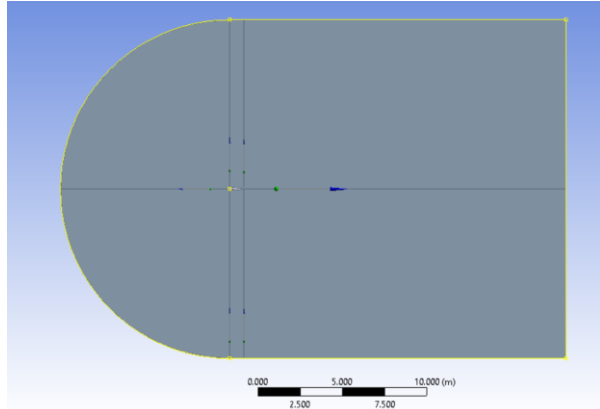


Figure 4.32 Drawing Wind tunnel for the airfoils' simulation

Due to the limited number of cells of the Ansys' student license and saving the calculation load of the computers, we could not create a mesh with an extremely large size to prevent the blockage effect. Hence, we would like to draw the wind tunnel by combining a semi-circle with 20 m diameter and a square with 20 m length. This 20 m length was much larger than the minimum 2.4 m to assure the blockage effect would not happen during our simulations. The mesh sizes of the three airfoils are shown below.

Airfoils	Cells	Faces	Nodes
Clark Y airfoil with 1 m chord length	240400	482002	241602
Skywalker X8's airfoil with 382 mm chord length	240000	481200	241200
Clark Y airfoil with 382 mm chord length	240000	481200	241200

Table 4.5 Mesh size of the airfoils

4.5.3. Model selection in Ansys Fluent

All simulations are under incompressible turbulent flow due to the calculation of their Reynolds numbers, which will be shown in sections 4.5.3 and 5.2. Therefore, the Spalart-Allmaras Turbulence Model had been chosen because it is mainly for aerodynamic flows. Since it requires that the dimensionless wall distance, y^+ value of the mesh should be smaller than 1, we did the calculation of the length of the first element of the edges in the mesh to ensure the y^+ value can be smaller than 1 in the next section.

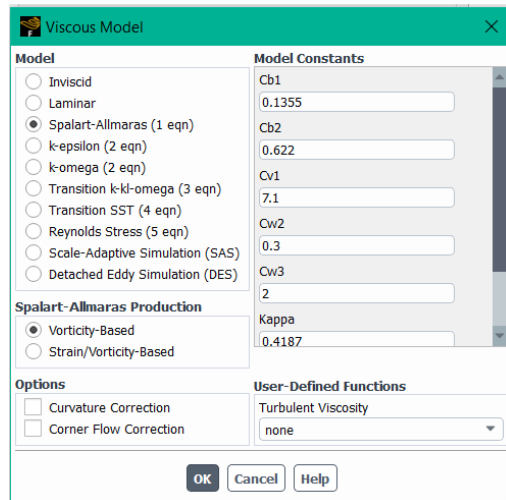


Figure 4.33 Spalart-Allmaras Model in Ansys Fluent

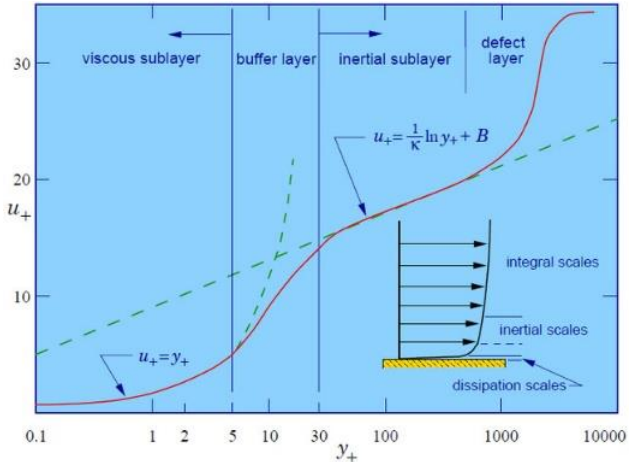


Figure 4.34 u^+ vs y^+ graph

4.5.4. Calculation of length of first element of the edge in mesh

For the calculation of the length of the first element of the mesh, we first had to define the value of y^+ first. From section 4.5.2, we assumed that the y^+ value should be smaller than 1 so we could use the S.A model for the simulation. Since we would like to compare our simulation results of the Clark Y airfoil with 1 m chord length to the Xfoil result with $Re = 1000000$, we set that the freestream velocity, $U_\infty = 14.9 \text{ ms}^{-1}$; density of the air, $\rho_\infty = 1.2 \text{ ms}^{-3}$; dynamic viscosity, $\mu = 0.00001788 \text{ kgm}^{-1}\text{s}^{-1}$; reference length = chord length = 1 m. According to the calculation below, we found that when the wall spacing was smaller than 0.0000235 m and the $Re = 1000000$, the y^+ value can be smaller than 1.

Input		Output	
<input type="button" value="Reset to Sea Level Conditions"/>		<input type="button" value="Compute Wall Spacing"/>	
$U_\infty:$	<input type="text" value="14.9"/>	$\Delta s:$	<input type="text" value="0.00002352879860611332"/>
freestream velocity (m/s)		wall spacing (m)	
$\rho:$	<input type="text" value="1.2"/>	$Re_x:$	<input type="text" value="999999.999999999"/>
freestream density (kg/m ³)		Reynolds number	
$\mu:$	<input type="text" value="0.00001788"/>	Note: -1 indicates an input error	
dynamic viscosity (kg/m s)			
$L:$	<input type="text" value="1.0"/>		
reference length (m)			
$y^+:$	<input type="text" value="1.0"/>		
desired y^+			

Figure 4.35 Calculation of the wall spacing referring to $y^+ = 1$ &

$$Re = 1000000 [18]$$

From Figure 4.36, the edges on the 1 m chord were approximately 10 m so the edge length for calculating the length of the first element in Figure 4.37 was 10 m.

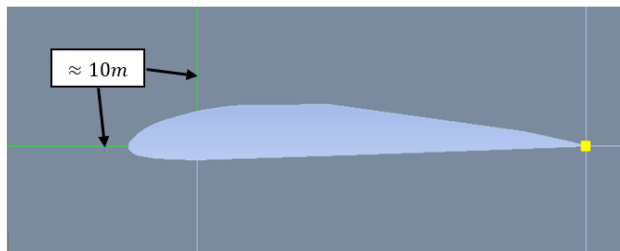


Figure 4.36 edges around the chord

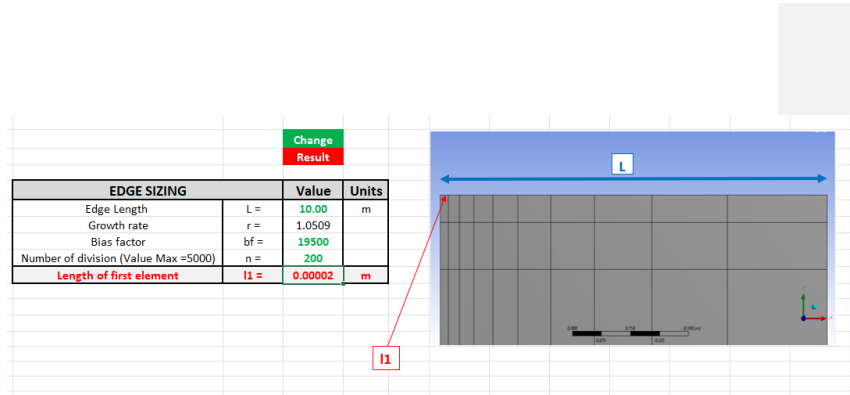


Figure 4.37 Calculation of the length of the first element

According to Figure 4.37, when the number of divisions = 200 and the bias factor = 19500, the length of the first element can be around 0.00002 m. Consequently, the edge sizing with the number of divisions = 200 and the bias factor = 19500 should be applied to the edges around the airfoil in its mesh.

4.5.5. Results of the dimensionless wall distances, y^+

We checked the y^+ values of each mesh by plotting the contour of the “Wall Yplus” of the airfoils after the simulation to ensure the y^+ values would be smaller than 1. For instance, referring to Figure 4.38 to 4.40, the y^+ values of all meshes of the airfoils could be smaller than 1 at 0 degree of AOA.

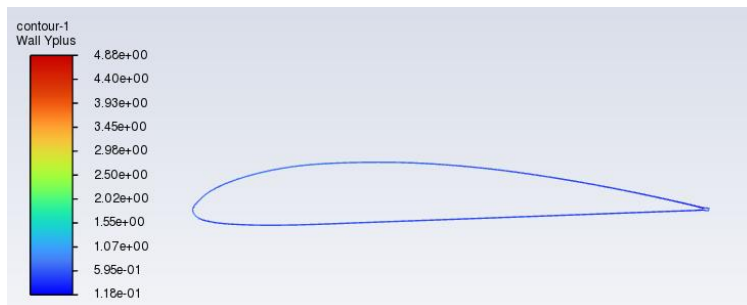


Figure 4.38 y^+ of the Clark Y airfoil with 1 m chord length at 0 deg of AOA

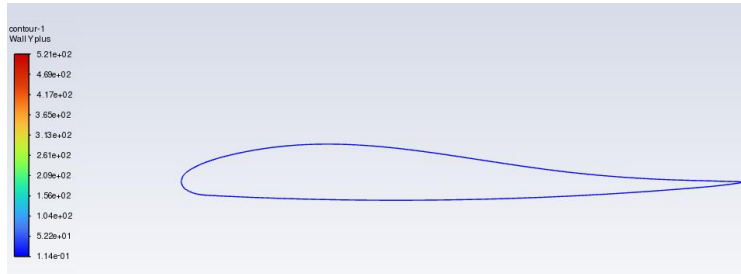


Figure 4.39 y^+ of the Skywalker X8's airfoil with 382 mm chord length at 0 deg of AOA

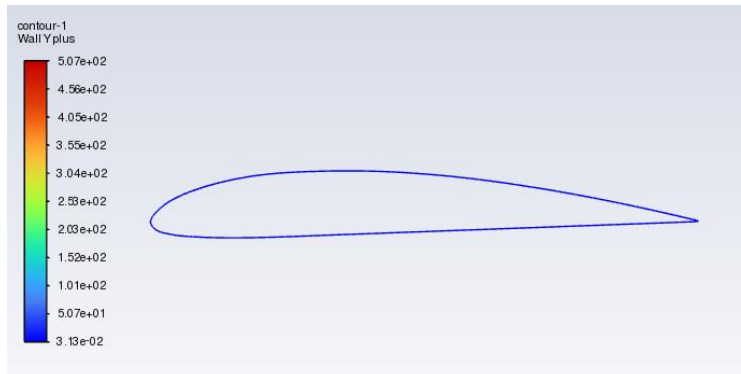


Figure 4.40 y^+ of the Clark Y airfoil with 382 mm chord length at 0 deg of AOA

4.5.6. Boundary conditions in Ansys Fluent

From section 4.5.3, the inlet velocity = 14.9 ms^{-1} for the Clark Y airfoil with 1 m chord length in order to set its $\text{Re} = 1000000$.

For the two airfoils with 382 mm chord length, their inlet velocities were set at 17.5 ms^{-1} because of the ITF project[1], our VTOL UAV should fly at a speed of 15 to 20 m/s. Hence, the inlet velocity was assumed at 17.5 ms^{-1} .

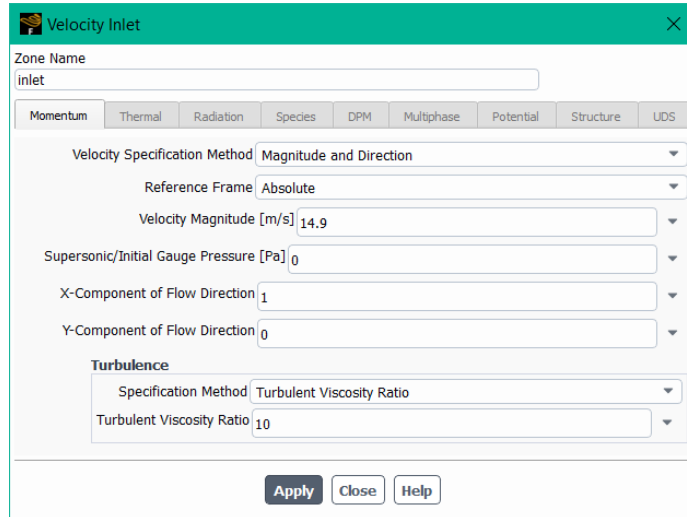


Figure 4.41 Inlet velocity setting in Ansys Fluent

For other parameters in the boundary conditions of all simulations in Ansys Fluent, we kept them as the default values. The examples of the boundary conditions of the three airfoils are shown below.

— Inlet	
— inlet	
Velocity Specification Method	Magnitude and Direction
Reference Frame	Absolute
Velocity Magnitude [m/s]	14.9
Supersonic/Initial Gauge Pressure [Pa]	0
Component of Flow Direction (x,y)	(0.9994, 0.0349)
Turbulent Specification Method	Turbulent Viscosity Ratio
Turbulent Viscosity Ratio	10
— Outlet	
— outlet	
Backflow Reference Frame	Absolute
Gauge Pressure [Pa]	0
Pressure Profile Multiplier	1
Backflow Direction Specification Method	Normal to Boundary
Turbulent Specification Method	Turbulent Viscosity Ratio
Backflow Turbulent Viscosity Ratio	10
Backflow Pressure Specification	Total Pressure
Build artificial walls to prevent reverse flow?	no
Average Pressure Specification?	no
Specify targeted mass flow rate	no

— airfoil	
Wall Motion	Stationary Wall
Shear Boundary Condition	No Slip
Wall Surface Roughness	0
Wall Roughness Height [m]	0
Wall Roughness Constant	0.5
— wall-surface_body	
Wall Motion	Stationary Wall
Shear Boundary Condition	No Slip
Wall Surface Roughness	0
Wall Roughness Height [m]	0
Wall Roughness Constant	0.5

Figure 4.42 & 4.43
 Boundary conditions of Clark Y airfoil with 1 m chord length at 2 deg of AOA with number of divisions = 200

— Inlet	
— inlet	
Velocity Specification Method	Magnitude and Direction
Reference Frame	Absolute
Velocity Magnitude [m/s]	17.5
Supersonic/Initial Gauge Pressure [Pa]	0
Component of Flow Direction (x,y)	(0.9976, 0.0698)
Turbulent Specification Method	Turbulent Viscosity Ratio
Turbulent Viscosity Ratio	10
— Outlet	
— outlet	
Backflow Reference Frame	Absolute
Gauge Pressure [Pa]	0
Pressure Profile Multiplier	1
Backflow Direction Specification Method	Normal to Boundary
Turbulent Specification Method	Turbulent Viscosity Ratio
Backflow Turbulent Viscosity Ratio	10
Backflow Pressure Specification	Total Pressure
Build artificial walls to prevent reverse flow?	no
Average Pressure Specification?	no
Specify targeted mass flow rate	no
— Wall	
— airfoil	
Wall Motion	Stationary Wall
Shear Boundary Condition	No Slip
Wall Surface Roughness	0
Wall Roughness Height [m]	0
Wall Roughness Constant	0.5
— wall-surface_body	
Wall Motion	Stationary Wall
Shear Boundary Condition	No Slip
Wall Surface Roughness	0
Wall Roughness Height [m]	0
Wall Roughness Constant	0.5

Figure 4.44 & 4.45
 Boundary conditions of Skywalker X8's airfoil with 382 mm chord length at
 4 deg of AOA with number of divisions = 200

— Inlet	
— inlet	
Velocity Specification Method	Magnitude and Direction
Reference Frame	Absolute
Velocity Magnitude [m/s]	17.5
Supersonic/Initial Gauge Pressure [Pa]	0
Component of Flow Direction (x,y)	(0.9976, 0.0698)
Turbulent Specification Method	Turbulent Viscosity Ratio
Turbulent Viscosity Ratio	10
— Outlet	
— outlet	
Backflow Reference Frame	Absolute
Gauge Pressure [Pa]	0
Pressure Profile Multiplier	1
Backflow Direction Specification Method	Normal to Boundary
Turbulent Specification Method	Turbulent Viscosity Ratio
Backflow Turbulent Viscosity Ratio	10
Backflow Pressure Specification	Total Pressure
Build artificial walls to prevent reverse flow?	no
Average Pressure Specification?	no
Specify targeted mass flow rate	no

— Wall	
— airfoil	
Wall Motion	Stationary Wall
Shear Boundary Condition	No Slip
Wall Surface Roughness	0
Wall Roughness Height [m]	0
Wall Roughness Constant	0.5
— wall-surface_body	
Wall Motion	Stationary Wall
Shear Boundary Condition	No Slip
Wall Surface Roughness	0
Wall Roughness Height [m]	0
Wall Roughness Constant	0.5

Figure 4.46 & 4.47
Boundary conditions of Clark Y airfoil with 382 mm chord length at 4 deg of AOA with number of divisions = 200

4.5.7. 2D airfoil simulation

During the simulations of the airfoils, the coefficients of lift, c_l and the coefficients of drag, c_d would be simulated at different angles of attack (AOA). We could simply change the x-component and the y component of the flow direction under the “Velocity Inlet” setting in Figure 4.41. Likewise, we should change the x-component and the y-component of the force vector in the lift and drag report definition too.

	x	y
Cl	(-1)*SIN(α)	COS(α)
Cd	COS(α)	SIN(α)
Inlet velocity	COS(α)	SIN(α)

Figure 4.48 x-component and the y-component of the force vector for the lift

and drag report definition and the inlet velocity (AOA in radians)

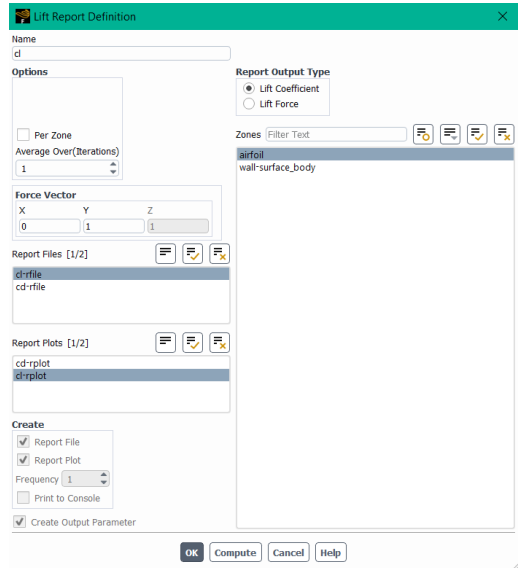


Figure 4.49 Lift report definition when AOA = 0 degree

We would like to find the c_l and c_d of the Clark Y airfoils (1 m chord length) when its AOA, $\alpha = 0, 2, 4, 6, 8$ and 10 degrees, while find the c_l/c_d ratio and the maximum c_l of the two smaller airfoils (382 mm chord length) when their AOA = $-4, -2, 0, 2, 4, 6, 8$, and 10 degrees. Then, we could plot the “ c_l vs AOA” graph, “ c_d vs AOA” graph and the “ c_l/c_d vs AOA” graph for the three airfoils respectively.

4.5.8. Convergence test

For the convergence test, we checked the convergence of solution of the simulation on the “Console” in Ansys Fluent. All the solution of our simulations could be converged and shown on the console.

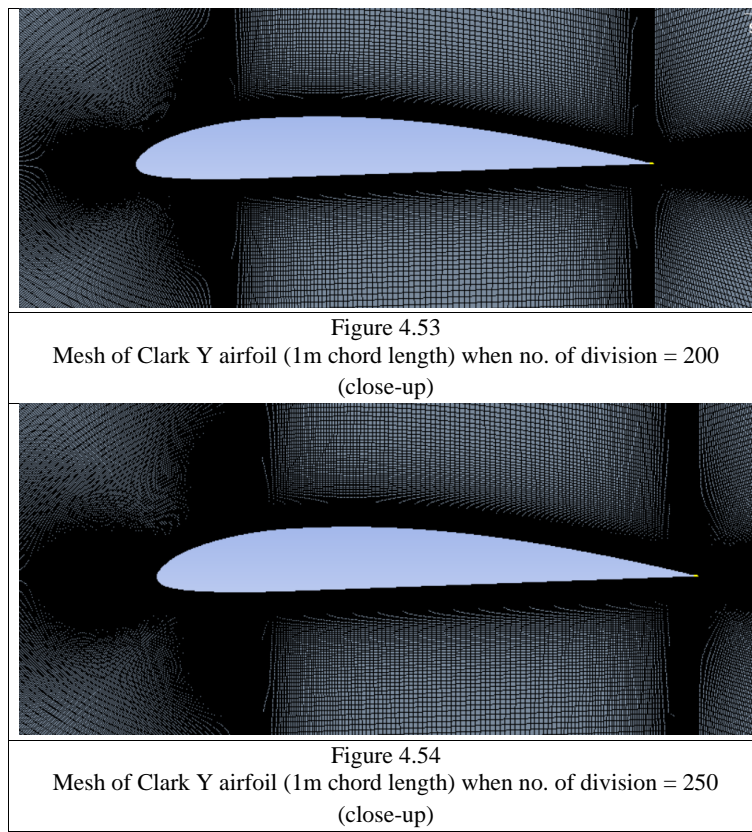
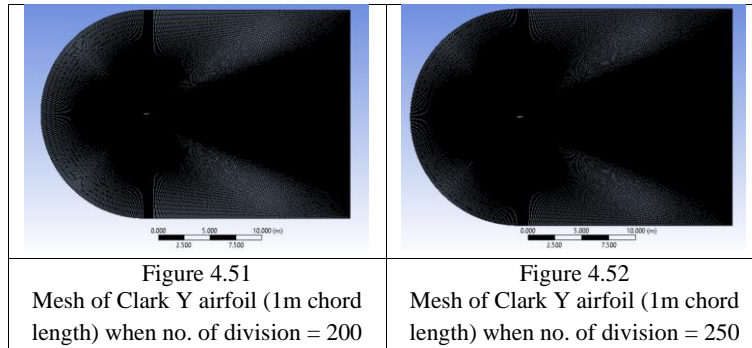
```
Console
296 1.1764e-06 7.2510e-12 6.3197e-13 1.6301e-10 3.7824e-01 1.2114e-02 0:07:00 704
297 1.1558e-06 7.1231e-12 6.2088e-13 1.6006e-10 3.7824e-01 1.2114e-02 0:07:56 703

iter continuity x-velocity y-velocity nut cl cd time/iter
298 1.1356e-06 6.9974e-12 6.0998e-13 1.5716e-10 3.7824e-01 1.2114e-02 0:08:40 702
299 1.1157e-06 6.8738e-12 5.9926e-13 1.5432e-10 3.7824e-01 1.2114e-02 0:09:16 701
300 1.0962e-06 6.7524e-12 5.8873e-13 1.5153e-10 3.7824e-01 1.2114e-02 0:07:24 700
301 1.0770e-06 6.6332e-12 5.7838e-13 1.4879e-10 3.7824e-01 1.2114e-02 0:08:15 699
302 1.0581e-06 6.5160e-12 5.6821e-13 1.4610e-10 3.7824e-01 1.2114e-02 0:08:55 698
303 1.0395e-06 6.4008e-12 5.5822e-13 1.4346e-10 3.7824e-01 1.2114e-02 0:07:07 697
304 1.0213e-06 6.2877e-12 5.4840e-13 1.4086e-10 3.7824e-01 1.2114e-02 0:08:00 696
305 1.0033e-06 6.1765e-12 5.3875e-13 1.3832e-10 3.7824e-01 1.2114e-02 0:08:43 695
306 9.8572e-07 6.0673e-12 5.2926e-13 1.3582e-10 3.7824e-01 1.2114e-02 0:09:16 694
306 solution is converged
Registering ReportDefFile, ("C:\Users\Athena\Documents\PolyU\FYP\CFD\Sim_files\Sim_files
\PolyU\FYP_CFD\Sim_files\Sim_files\dp0\FFF\Fluent\", \cl-rfile.out")
Writing data to C:\Users\Athena\Documents\PolyU\FYP\CFD\Sim_files\Sim_files\dp0\FFF\Fluen
x-coord
y-coord
pressure
x-velocity
y-velocity
nut
Done.
Calculation complete.
```

Figure 4.50 Capture of the converged results of the Clark Y airfoil (1 m chord length) at 0 deg of AOA

4.5.9. Grid independence test

For the grid independence test, we compared the results of the simulations in the different numbers of divisions of the edges of the meshes. We kept the bias factor and increased the number of divisions to 250. The number of grids in the mesh will be increased when the number of divisions increases. The two meshes whose number of divisions are 200 and 250 are shown below.



Then, we repleted the simulations at different AOA by using the new mesh. The simulation results of the 2 meshes are shown below.

angle(α)	Cl	Cd
0	3.78E-01	1.21E-02
2	5.94E-01	1.29E-02
4	8.06E-01	1.42E-02
6	1.01E+00	1.60E-02
8	1.21E+00	1.85E-02
10	1.384888	0.02183096

Figure 4.55
Results of the Clark Y airfoil (1m chord length) when no. of division of its mesh = 200

angle(α)	Cl	Cd
0	3.75E-01	1.21E-02
2	5.95E-01	1.29E-02
4	8.11E-01	1.42E-02
6	1.02E+00	1.60E-02
8	1.22E+00	1.85E-02
10	1.397451	0.02189205

Figure 4.56
Results of the Clark Y airfoil (1m chord length) when no. of division of its mesh = 250

Referring to the above results, the differences between the two simulation results are smaller than 1%. Hence, this showed that the grid independence test of the Clark Y airfoil with 1 m chord length was done. The simulation result would not be affected much when the number of divisions of the mesh is larger than 200. For saving time and calculating load during the simulation, we would like to remain the number of divisions of the mesh to 200.

4.6. Manufacturing of the composited wings

4.6.1. Composited wings design

For our composited VTOL UAV, we would like to keep the polystyrene fuselage and manufacturing a pair of composited wings for it. As this was a reinforcement of the original wings, the wing span, the sweep angle, the root rib and the wing tip should be similar to the original Skywalker X8. This also ensured that the composited wings could be assembled with the original polystyrene fuselage by the orange connection part in section 4.2.2.

Besides, there was a transition part from the original Skywalker X8's airfoil to the Clark Y airfoil for assembling the new composited wings with the fuselage. Therefore, this transition part of 50 mm width was located at the root rib of the wings. The airfoils within this transition part were not consistent because this part was built by the loft function in SolidWorks for connecting the original airfoil of Skywalker X8 and the Clark Y airfoil.

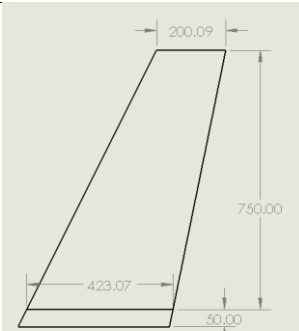


Figure 4.57 Dimensions of a
composed wing



Figure 4.58 CAD drawing of a
composed wing

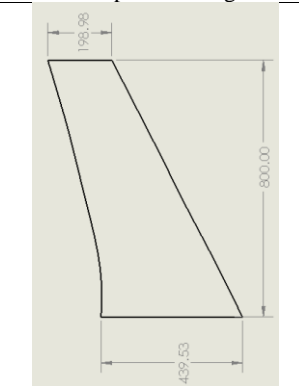


Figure 4.59
Dimensions of a Skywalker X8's
wing (without connection with
winglet)

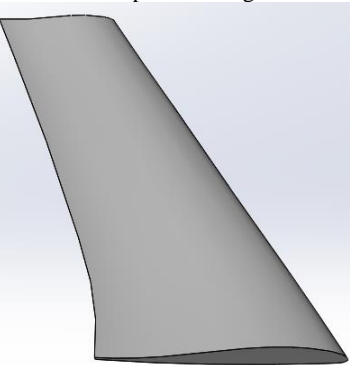


Figure 4.60
CAD drawing of a Skywalker X8's
wing (without connection with winglet)

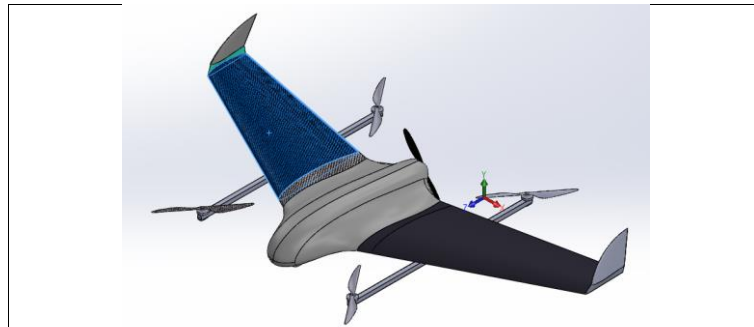


Figure 4.61 VTOL UAV with composited wings (made of carbon fibre)

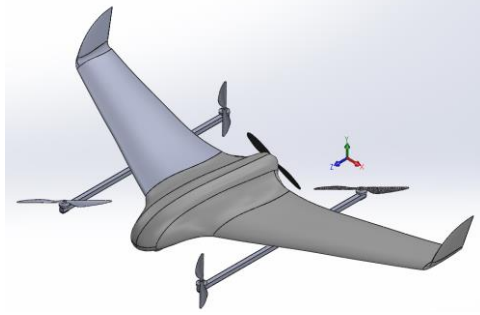


Figure 4.62 VTOL UAV with original wings (made of polystyrene)

4.6.2. Mold design for the composited wings

To get a pair of stronger composited wings, there were no plywood ribs would be stuck between the composited skin of the wings. Different from the traditional plywood ribs, the internal composted stringers could provide stronger mechanical strength as the ribs were made during the manufacturing of the wings.

From the flowchart for manufacturing of composited wings in section 4.1.2, each mold should be covered by 2 layers of 3K carbon fiber sheets. Hence, the thickness of the walls of each mold can become the composited ribs after the combining them by covering 2 more layers of 3K carbon fiber sheets. As the thickness of a 3K carbon fiber sheet is around 0.2mm, the distance of the mold to the next mold should be 0.8 mm.

For a better appearance and more accurate dimensions of the composited parts, 5 mm width of extensions at the two ends of the molds were designed. The extra 5 mm extensions could be simply trimmed after the manufacturing process for getting good edges for each mold.

It is suggested that the holes for installing the servo motors and the elevons should be cut or drilled after finishing the manufacturing process. This could reduce the difficulties during the manufacturing process and debagging of the molds.

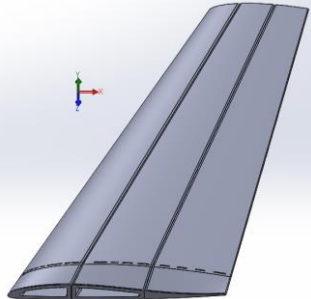
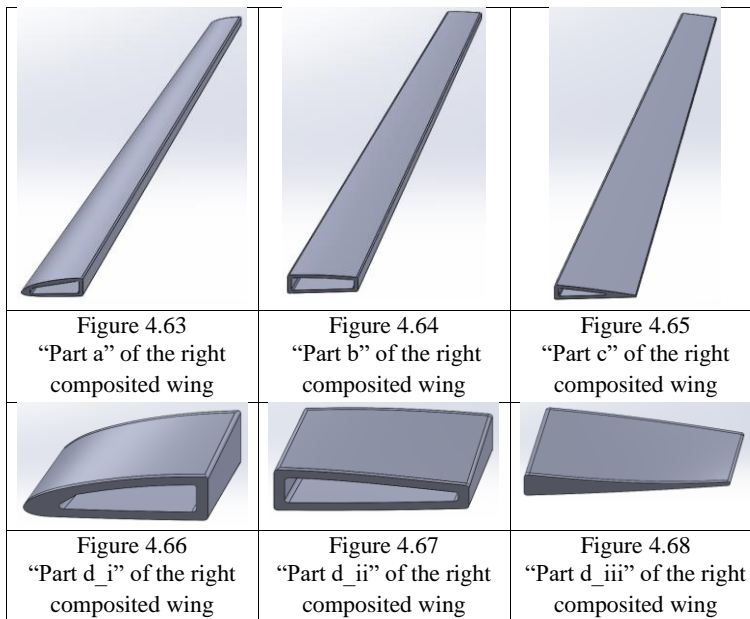
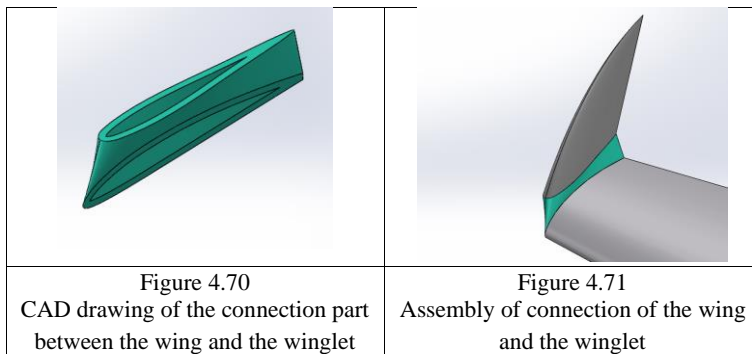


Figure 4.69 Combination of 6 molds of a composited wing

4.6.3. Connection of winglet and wing design

Concerning the difficulties of making a curve carbon fibre part, the connection between the wing and the winglet would not be made of carbon fibre. Hence, the original winglets are kept, and the connection part would be manufacturing by 3D printing. The CAD drawing of the connection part and the assembly are shown below.



Since a 3D printing part will be heavier than a carbon fiber part, the volume of the connection would like to be saved as low as possible. Therefore, the connection was designed to become a hollow part for reducing the weight.

4.6.4. Manufacturing process

4.6.4.1 Construction of Carbon Fibre mold

To form the shape of the wing, carbon fiber fabric was laid on the mold surface.

But before that, mold release wax and release agent film were applied to the mold successively to minimize the damage to the product during mold releasing.

After that, adhesive aerosol was sprayed on the mold. Adhesive aerosol is a strong glue so the carbon fiber fabric can be stuck to the shape of the mold. To strengthen the product, we used the second layer of carbon fiber to cover the first layer with the same approach. However, the junction of the second layer should be different from that of the first layer for ensuring its hardness.

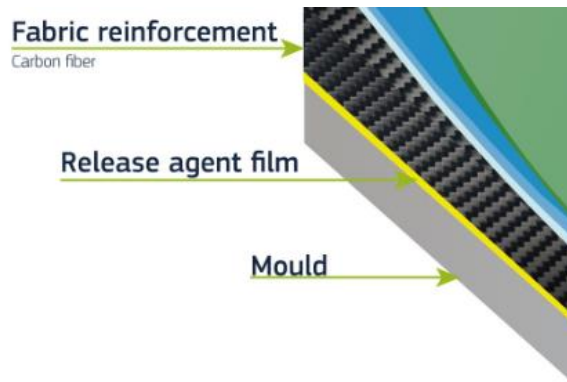


Figure 4.72 Cross section of the carbon fiber mold layers[19]

The wing mold is separated into 6 parts and each part has bonding surfaces to stick with each other. When laying a single mold with carbon fiber fabric, the seam of the fabric should be on such surfaces so that when the parts are combined together the wing surface would be smooth and would not cause interference to the aerodynamic performance of the wing.



Figure 4.73 Lay up of carbon fiber fabric, where seam located in the bonding surfaces

In order to further strengthen the structure of the CF wing, epoxy resin is used to permeate and cover the carbon fiber. In this project, the epoxy resin was formulated by 105 epoxy resin and 209 hardener with ratio of 40:11. To apply the epoxy resin to the carbon fiber, two methods – vacuum infusion and wet layup were both attempted in this project.

4.6.4.2 Vacuum Infusion

For vacuum infusion, vacuum film is used to make the vacuum bag. Since the mold was hollow, there were outer and inner vacuum bags to surround the outer and inner surface of the mold respectively to prevent the epoxy resin from entering the hollow. Otherwise, the debagging of the composited parts could not be done easily or even successfully. Before the bags were sealed, the resin flowing setup was collocated.

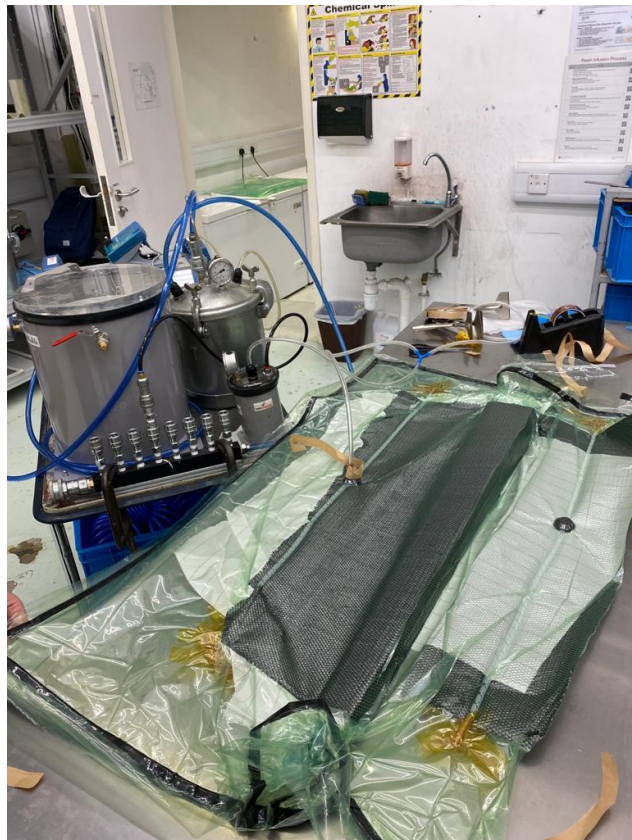


Figure 4.74 Setup of vacuum infusion

As shown in the Figure 4.74, a large piece of white peel ply was placed under the 3D printing mold and the mold was placed in the middle. Then, two pieces of the flow media (black with net structure) were placed under the peel ply on the two sides respectively. It should be noticed that the flow media were not allowed to touch the mold. If this happens, an uneven flow of resin would occur. This can cause the failure of the vacuum infusion as some parts of the carbon fiber fabric may not be filled by the resin. Finally, there were flow channels and end plugs on both sides of the peel ply for resin induction.



Figure 4.75 Infusion of epoxy resin

After the vacuum bags were sealed, they were vacuumed by a vacuum pump through one of the end plugs. When the pressure inside the bags became 0 mbar, we inserted a tube that connected another end plug and a cup of epoxy resin. Due to the pressure difference, the epoxy resin would be sucked into the bag and flow through the mold. Since there was a size difference along the mold plus the end plugs were in the middle, the flow rate across the mold was not unanimous. However, it did not affect the process and the product quality because the setup was proper, we just needed to wait longer for the complete flow.



Figure 4.76 Completion of infusion

Once the mold was completely filled with epoxy resin, we could stuff the end plugs, remain at the 0-mbar pressure setting and wait for the carbon fiber fabric to harden on its mold which usually takes around 24 to 48 hours. Eventually, we removed the vacuum bags and released the product from the mold.

4.6.4.3 Wet Layup

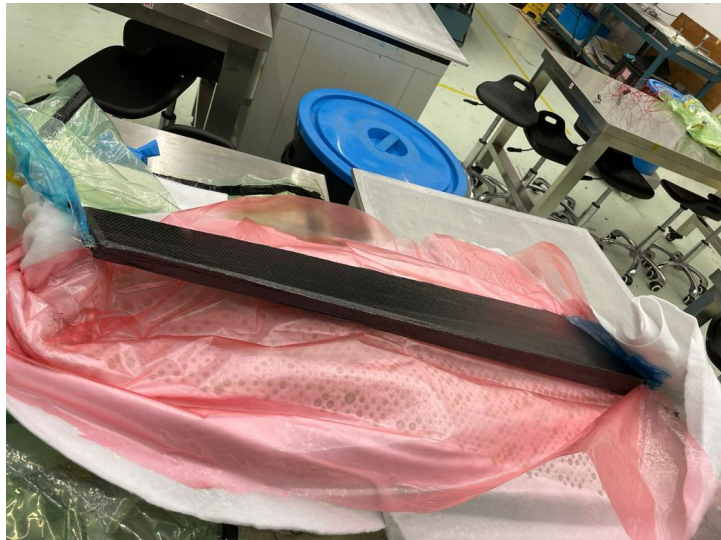


Figure 4.77 Layup of the CF mold



Figure 4.78 Wet layup method with vacuum assisted molding

Since the hollow of one of the molds was too small, the inner vacuum bag could not pass through it. Consequently, we decided to use the wet layup for the CF process. First, we directly smeared the CF mold with epoxy resin for at least 2 layers. Then, we laid the mold with PET release film for easier release from the outside layers. The PET release film used in this process has many small holes so that the exceed epoxy resin can be discharged. After, we laid it with a cloth and sealed the mold with vacuum bag.

To conduct the vacuuming, there were also a pressure indicator and a connector connected with the vacuum pump. The pressure should remain -28 inHg in the whole process. Meanwhile, the exceeded epoxy resin passed through the PET release film and was absorbed by the cloth. Finally, the epoxy resin dried evenly on the CF surface. The carbon fiber product should also be waited for 24 to 48 hours before the debagging process to assure the smeared resin was totally dried.

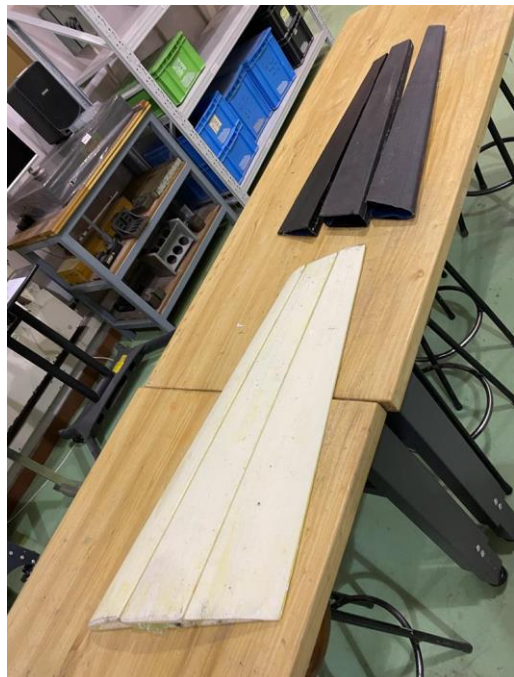


Figure 4.79 CF wing parts released from the molds

5. Chapter 5: Experimental results and Discussions

5.1. Flight log analysis of the flight test of VTOL Skywalker X8 UAV without payload

5.1.1. Total hovering time during flight test

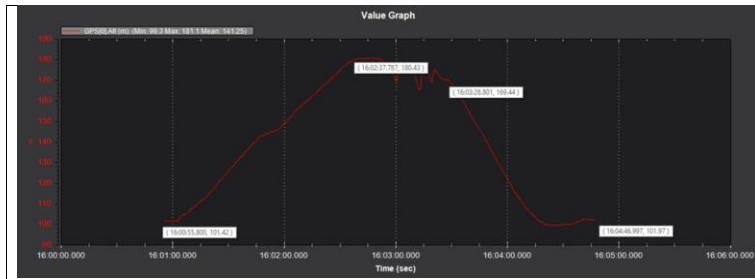


Figure 5.1 Altitude graph of the flight test

Some useful information was collected from the flight logs after the flight test of the VTOL Skywalker X8 UAV without its payload, the air quality sensor. From the figures above, the total time of one of the flights was around 4 minutes in total. Besides, the VTOL Skywalker X8 UAV spent around one and a half minutes doing the take-off and landing respectively. In final, the valid hovering time on that flight was around three minutes. This showed that without payload, the VTOL UAV required around three minutes to do the vertical take-off and landing.

5.1.2. Total cruising time during flight test

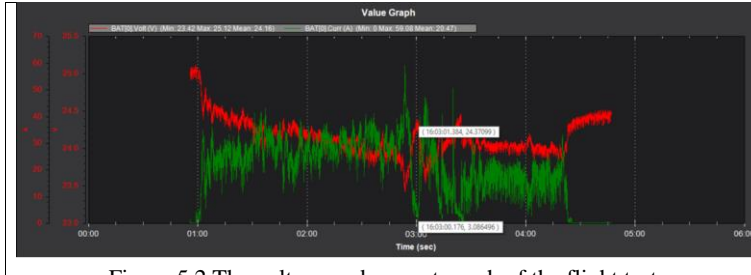


Figure 5.2 The voltage and current graph of the flight test

The graph above shows the voltage and the current every second respectively.

To estimate the cruising time, from Figure 5.1, a point on time equal to 16:03 was picked. At that time, the voltage and current were measured as 24.37099V and 3.086496A respectively. It is assumed that the current used an hour is = 3.08649Ah The power consumed an hour:

$$V * Ah = 24.37099 \times 3.086496 = 75.22Wh.$$

Assume the average voltage of the battery = 22.2 V.

$$\text{Required mAh of the battery} = \frac{75.22}{22.2} \times 1000 = 3388.29 \text{ mAh}$$

Therefore, to fly the VTOL UAV for an hour, a battery which has a capacity of 3388.29 mAh or above should be needed. As the battery that we used during this flight test was 16000 mAh, it is enough for our VTOL UAV to fly for about an hour.

5.1.3. General flight performance of VTOL Skywalker X8 UAV

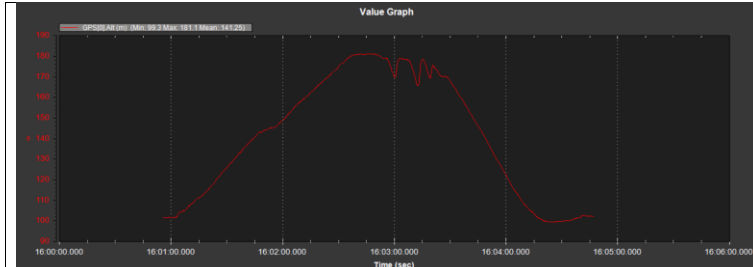


Figure 5.1: Altitude graph of the flight test

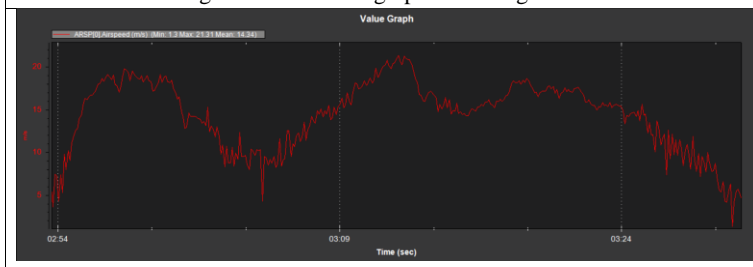


Figure 5.3 Speed graph of the flight test

From the above graphs, some performances of this flight can be concluded. First, Figure 5.1 shows the altitude graph of the GPS. Hence, the maximum altitude that the VTOL Skywalker X8 UAV flew is

$$ALT_{max} = 181.1 - 100 = 81.1 \text{ m}$$

Also, the average altitude that it flew during its cruising is

$$ALT_{avg} = 176.32 - 100 = 76.32 \text{ m}.$$

Both flight altitudes above were closed to 100 m, which is one of the objectives of the ITF project [1]. Since this was a flight test of testing the ability of the flying of the VTOL UAV, reaching the maximum flight altitude was not the main goal.

Figure 5.3, which is representing the speed curve during the hovering time. The magnitude of the average velocity on that flight was 14.34 ms^{-1} and the maximum speed is 21.31 ms^{-1} . According to the given data of the graph, the total horizontal distance that the VTOL Skywalker X8 UAV flew can be estimated. The estimated distance that it travelled during this flight test: $14.34 \times 60 = 806.4 \text{ m}$.

5.2. Simulation results in CFD

After each simulation in Ansys fluent, we could check three graphs: the residuals graph, the c_l graph, and the c_d graph. The residuals graph could show the function of error in the model. Therefore, a smaller value of the residual could provide a better simulation result. Clearly, the c_l graph and the c_d graph could prove the c_l value and the c_d values with respect to the desired AOA. The examples of the residuals graph, the c_l graph, and the c_d graph from the simulation result are shown below:

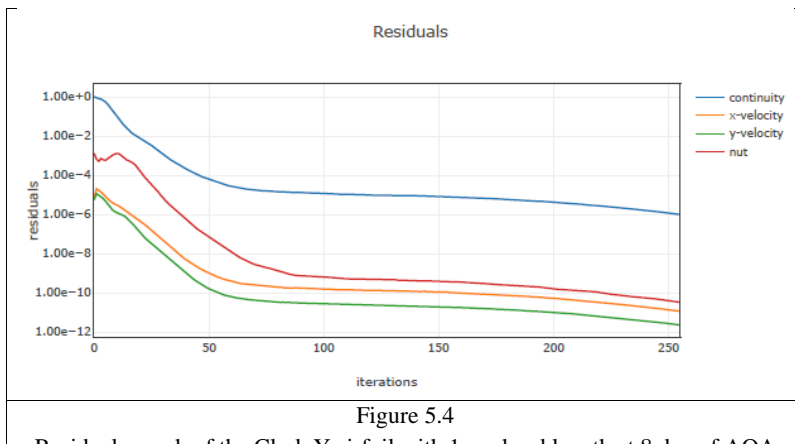
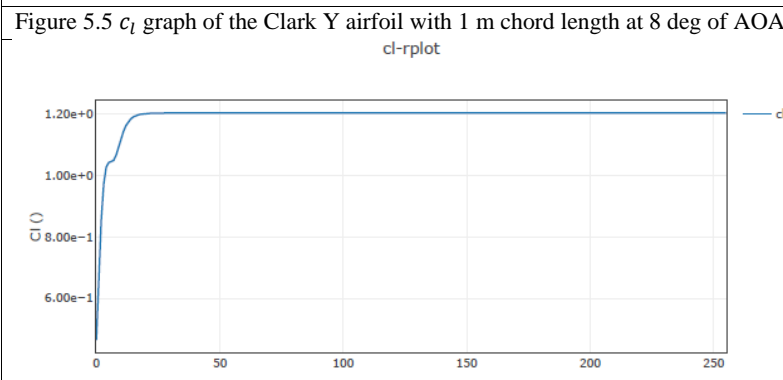
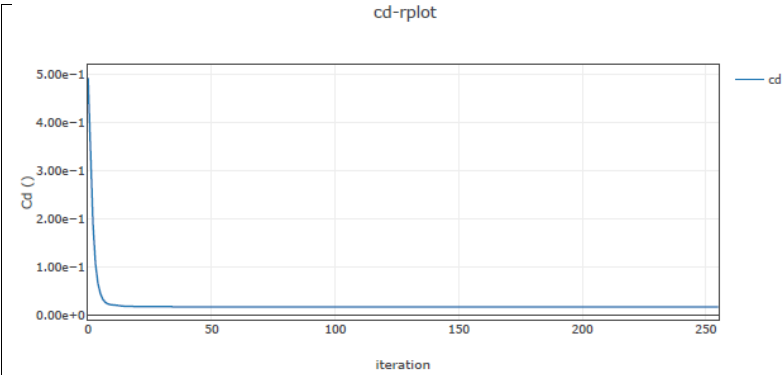


Figure 5.4
Residuals graph of the Clark Y airfoil with 1 m chord length at 8 deg of AOA



5.2.1. Comparison of the simulation and the Xfoil prediction of Clark Y airfoil

To compare the simulation results with the Xfoil prediction in $\text{Re} = 1000000$, its boundary condition followed the data in section 4.5.

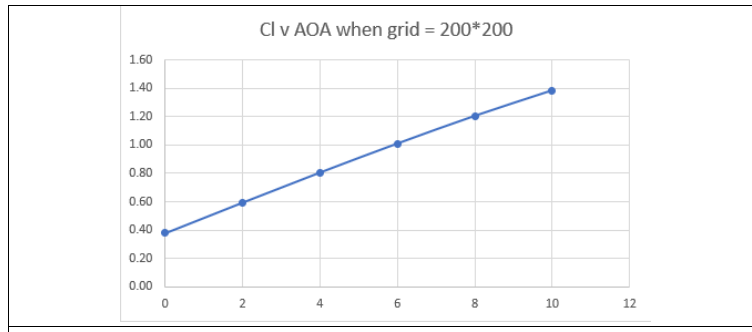


Figure 5.7
 c_l vs AOA graph of the Clark Y airfoil (1 m chord length) by simulations

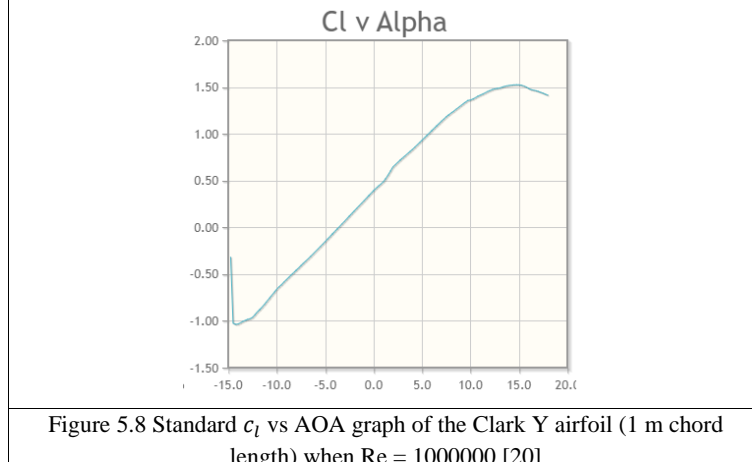


Figure 5.8 Standard c_l vs AOA graph of the Clark Y airfoil (1 m chord length) when $\text{Re} = 1000000$ [20]

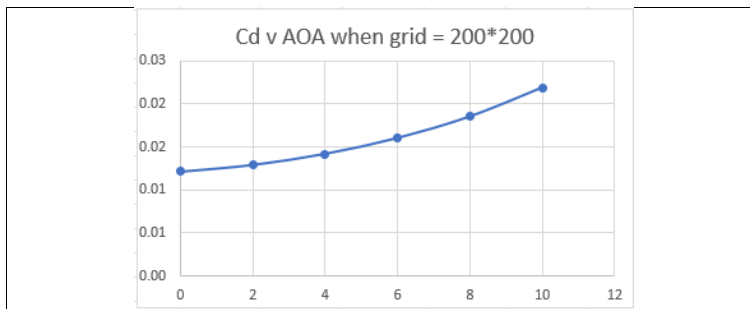


Figure 5.9 c_d vs AOA graph of the Clark Y airfoil (1 m chord length) by simulations

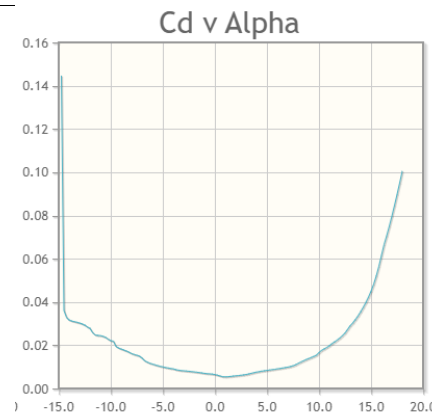


Figure 5.10
Standard c_d vs AOA graph of the Clark Y airfoil (1 m chord length) when $Re = 1000000$ [20]

From the above results, it showed that when the AOA was from 0 degree to 10 degrees, our simulation of the Clark Y airfoil with 1 m chord length could have similar results to the XFOIL standard data. Thus, our simulation setting could be proved, and we would like to use the same method to do the simulations for the Skywalker X8's airfoil and the Clark Y airfoil with a 382 mm chord length.

5.2.2. 2D simulation results of the airfoils

Assume the inlet velocity = 17.5 ms^{-1} ; density of the air, $\rho_\infty = 1.2 \text{ ms}^{-3}$; dynamic viscosity, $\mu = 0.00001788 \text{ kgm}^{-1}\text{s}^{-1}$; reference length = chord length = 382 mm. Thus, the Reynolds number of the simulations is shown below.

$$Re = \frac{\rho_\infty U_\infty L}{\mu} = \frac{1.2 * 17.5 * 0.382}{0.00001788} = 448657.72$$

angle(α)	C _I	C _d	C _I /C _d
-4	-1.64E-01	5.77E-03	-2.84E+01
-2	-8.06E-02	5.08E-03	-1.59E+01
0	3.59E-03	4.61E-03	7.79E-01
2	8.75E-02	4.33E-03	2.02E+01
4	1.71E-01	4.28E-03	4.00E+01
6	2.53E-01	4.52E-03	5.61E+01
8	3.33E-01	5.16E-03	6.46E+01
10	0.4080075	0.006447519	6.33E+01

Table 5.1
Simulation results of Skywalker X8's airfoil with 382 mm chord length

angle(α)	C _I	C _d	C _I /C _d
-4	-2.91E-02	5.28E-03	-2.84E+01
-2	5.11E-02	4.92E-03	-1.59E+01
0	1.31E-01	4.77E-03	2.75E+01
2	2.11E-01	4.83E-03	4.36E+01
4	2.89E-01	5.10E-03	5.67E+01
6	3.64E-01	5.60E-03	6.50E+01
8	4.35E-01	6.44E-03	6.76E+01
10	5.00E-01	7.74E-03	6.46E+01

Table 5.2
Simulation results of Clark Y airfoil with 382 mm chord length

C_l v AOA when grid = 200*200
(Skywalker X8)

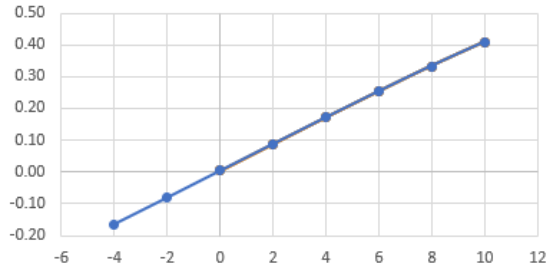


Figure 5.11
 c_l vs AOA graph of the Skywalker X8's airfoil (382 mm chord length)

C_l v AOA when grid = 200*200 (Clark Y airfoil)

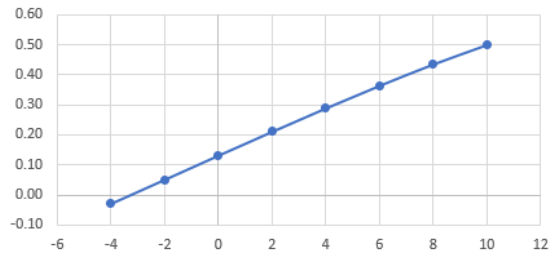


Figure 5.12 c_l vs AOA graph of the Clark Y airfoil (382 mm chord length)

C_d v AOA when grid = 200*200
(Skywalker X8)

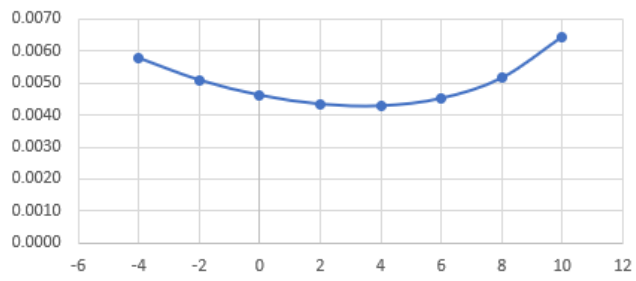


Figure 5.13
 c_d vs AOA graph of the Skywalker X8's airfoil (382 mm chord length)

C_d v AOA when grid = 200*200
(Clark Y airfoil)

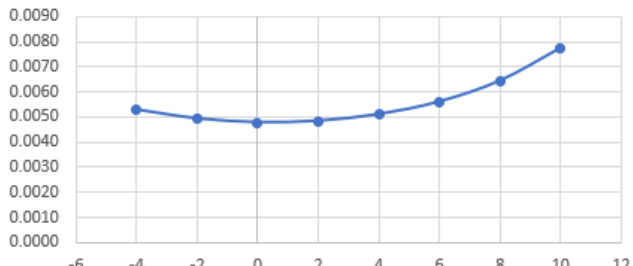


Figure 5.14 c_d vs AOA graph of the Clark Y airfoil (382 mm chord length)

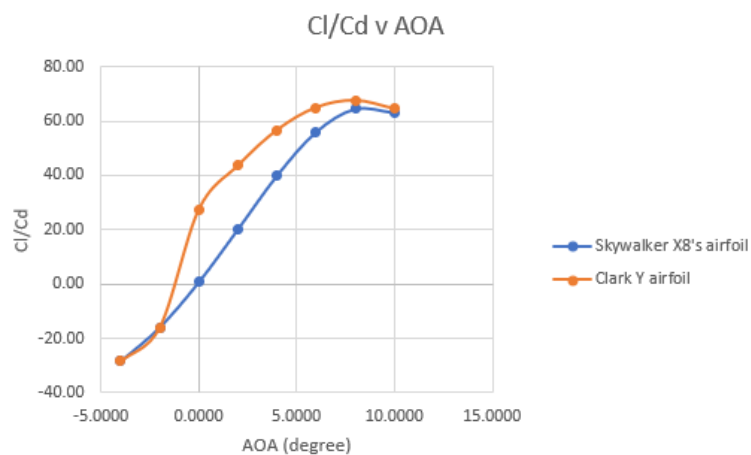


Figure 5.15
 c_l/c_d vs AOA graph of Skywalker X8's airfoil and Clark Y airfoil (chord lengths = 382 mm)

From Fig 5.15, obviously, when AOA = 0° to 10°, the c_l/c_d ratio of the Clark Y airfoil is higher than that of the Skywalker X8's airfoil. Besides, from Figure 5.11 and Figure 5.12, the Clark Y airfoil has higher maximum c_l than that of the Skywalker X8's airfoil. Consequently, the aerodynamics performance of the Clark Y airfoil can be better than that of the Skywalker X8. This showed that the Clark Y airfoil can be a good choice for our composited wings.

5.2.3. Application of lifting line theory with the 2D simulation results

From section 5.2.2, when $c_l = 0$, the approximated AOA of the Skywalker X8's airfoil = -0.02° while the approximated AOA of the Clark Y airfoil = -0.8°. Hence, the zero-lift AOA, $\alpha_{L=0}$ of the Skywalker X8 = -0.02°, while the zero-lift AOA, $\alpha_{L=0}$ of the Clark Y airfoil = -0.8°.

Excluding the transition part of the composited wing, we would like to use the zero-lift AOA of the two airfoils to estimate the coefficient of lift of the two wings, C_L by lifting line theory. Assumed there is no geometric twist. To apply the lifting line theory, we need the following Parameters:

Parameters	Skywalker X8's airfoil	Clark Y airfoil
Wing span, b	$750*2 = 1600 \text{ mm}$	$750*2 = 1600 \text{ mm}$
Wing root chord, c_r	423 mm	423 mm
Wing tip chord, c_t	198 mm	200 mm
Taper ratio, $\lambda = c_t/c_r$	$\frac{198}{423} = 0.468$	$\frac{200}{423} = 0.473$
Wing area, S	$0.5*(423+198)*800*2 = 496800 \text{ mm}^2$	$0.5*(423+200)*800*2 = 498400 \text{ mm}^2$
Aspect ratio, $AR = \frac{b^2}{S}$	$\frac{1600^2}{496800} = 5.15$	$\frac{1600^2}{498400} = 5.14$
Zero lift AOA, $\alpha_{L=0}$	$-0.02^\circ = -0.0003 \text{ rad}$	$-0.8^\circ = -0.0140$

Table 5.3 Required parameters for calculating the C_L by lifting line theory

By the following equations:

$$a_0 = 2\pi \text{ (By thin airfoil theory)}$$

$$c(\phi) = c_r[1 + (\lambda - 1)\cos\phi]$$

$$S = \frac{1}{2}(c_t + c_r)b = \frac{1}{2}c_r(1 + \lambda)b$$

$$AR = \frac{b^2}{S} = \frac{2b}{c_r(1 + \lambda)} \Rightarrow b = \frac{ARc_r(1 + \lambda)}{2}$$

$$\begin{aligned} \Rightarrow \mu_{SkywalkerX8} &= \frac{ca_0}{4b} = \frac{a_0}{2(1 + \lambda)AR} [1 + (\lambda - 1)\cos\phi] \\ &= 0.4155(1 - 0.532\cos\phi) \end{aligned}$$

$$\begin{aligned} \Rightarrow \mu_{ClarkY} &= \frac{ca_0}{4b} = \frac{a_0}{2(1 + \lambda)AR} [1 + (\lambda - 1)\cos\phi] \\ &= 0.4149(1 - 0.527\cos\phi) \end{aligned}$$

Substituting the above parameters into the monoplane equations of the Skywalker X8's airfoil and the Clark Y airfoil:

$$\begin{aligned}
 & \mu_{SkywalkerX8}(\alpha - \alpha_{L=0}) \sin\phi \\
 &= A_1 \sin\phi (\mu_{SkywalkerX8} + \sin\phi) \\
 &+ A_3 \sin 3\phi (3\mu_{SkywalkerX8} + \sin\phi) \\
 &+ A_5 \sin 5\phi (5\mu_{SkywalkerX8} + \sin\phi) \\
 &+ A_7 \sin 7\phi (7\mu_{SkywalkerX8} + \sin\phi)
 \end{aligned}$$

$$\begin{aligned}
 & \mu_{ClarkY}(\alpha - \alpha_{L=0}) \sin\phi \\
 &= A_1 \sin\phi (\mu_{ClarkY} + \sin\phi) + A_3 \sin 3\phi (3\mu_{ClarkY} + \sin\phi) \\
 &+ A_5 \sin 5\phi (5\mu_{ClarkY} + \sin\phi) + A_7 \sin 7\phi (7\mu_{ClarkY} + \sin\phi)
 \end{aligned}$$

As there are four unknowns, A_1, A_3, A_5, A_7 for each monoplane equation, we can pick 4 arbitrary φ values, $22.5^\circ, 45^\circ, 67.5^\circ$, and 90° ($0.3927, 0.7854, 1.1781$, and 0.1508 in radians) and substitute them into the monoplane equations.

For the monoplane equation of the Skywalker X8's airfoil:

When $\alpha = 0^\circ = 0 \text{ rad}$, $\phi = 22.5^\circ = 0.3927 \text{ rad}$,

$$\begin{aligned}\mu_{\text{SkywalkerX8}} &= 0.4155(1 - 0.532 \cos(0.3927)) = 0.2113 \\ \mu_{\text{SkywalkerX8}}(0 - (-0.0003)) \sin(0.3927) &= 2.42584 \times 10^{-5} \\ \therefore 2.43 \times 10^{-5} &= A_1 \sin(0.3927)(0.2113 + \sin(0.3927)) \\ &\quad + A_3 \sin[3(0.3927)](3 * 0.2113 + \sin(0.3927)) \\ &\quad + A_5 \sin[5(0.3927)](5 * 0.2113 + \sin(0.3927)) \\ &\quad + A_7 \sin[7(0.3927)](7 * 0.2113 + \sin(0.3927)) \\ &= 0.2273A_1 + 0.9391A_3 + 1.3295A_5 + 0.1724A_7\end{aligned}$$

\therefore Similarly, at the AOA = 0, 2, 4, 6, 8, and 10 degrees, the values of $\mu_{\text{SkywalkerX8}}$, $\mu_{\text{SkywalkerX8}}(\alpha - \alpha_{L=0}) \sin \phi$, and the coefficients of A_1 , A_3 , A_5 , and A_7 values of the monoplane equations are shown below:

φ (°)	α (°)	μ	$\mu(\alpha - \alpha_{L=0})\sin\phi$
22.5	0	0.2113	0.0000243
45	0	0.2592	0.0000550
67.5	0	0.3309	0.0000917
90	0	0.4155	0.0001247
22.5	2	0.2113	0.0028466
45	2	0.2592	0.0064527
67.5	2	0.3309	0.0107634
90	2	0.4155	0.0146283
22.5	4	0.2113	0.0056689
45	4	0.2592	0.0128503
67.5	4	0.3309	0.0214350
90	4	0.4155	0.0291320
22.5	6	0.2113	0.0084912
45	6	0.2592	0.0192480
67.5	6	0.3309	0.0321067
90	6	0.4155	0.0436357
22.5	8	0.2113	0.0113135
45	8	0.2592	0.0256457
67.5	8	0.3309	0.0427783
90	8	0.4155	0.0581394
22.5	10	0.2113	0.0141358
45	10	0.2592	0.0320434
67.5	10	0.3309	0.0534500
90	10	0.4155	0.0726431

Table 5.4
Values of $\mu_{SkywalkerX8}$ & $\mu_{SkywalkerX8}(\alpha - \alpha_{L=0})\sin\phi$ at different AOA

φ (°)	μ	Coefficient of A_1	Coefficient of A_3	Coefficient of A_5	Coefficient of A_7
22.5	0.2113	0.2273	0.9391	1.3295	0.7124
45	0.2592	0.6833	1.0498	-1.4164	-1.7830
67.5	0.3309	1.1593	-0.7335	-0.9867	2.9936
90	0.4155	1.4155	-2.2465	3.0775	-3.9085

Table 5.5

Coefficients of $\mu_{\text{Skywalker X8}}$ & A_1, A_3, A_5 , and A_7 values at different φ

Solving the A_1, A_3, A_5 , and A_7 by Gaussian elimination,

α (°)	A_1	A_3	A_5	A_7
0	0.00008	0.00000	0.00000	0.00000
2	0.00979	0.00019	0.00035	-0.00003
4	0.01949	0.00038	0.00070	-0.00007
6	0.02920	0.00057	0.00104	-0.00010
8	0.03890	0.00076	0.00139	-0.00013
10	0.04861	0.00095	0.00174	-0.00016

Table 5.6 A_1, A_3, A_5 , and A_7 at different AOA (Skywalker X8's airfoil)

As $C_L = A_1 \pi AR$,

α (°)	C_L
0	0.0013
2	0.1583
4	0.3152
6	0.4722
8	0.6291
10	0.7861

Table 5.7 C_L values at different AOA (Skywalker X8's airfoil)

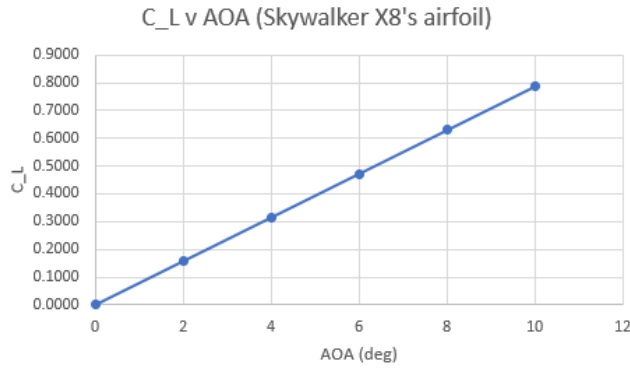


Figure 5.16
 C_L v AOA graph of the Skywalker X8's airfoil with 382 mm chord length

Similarly, at the AOA = 0, 2, 4, 6, 8, and 10 degrees, the values of μ_{ClarkY} , $\mu_{ClarkY}(\alpha - \alpha_{L=0})\sin\phi$, and the coefficients of A_1 , A_3 , A_5 , and A_7 values of the monoplane equations are shown below:

φ (°)	α (°)	μ	$\mu(\alpha - \alpha_{L=0})\sin\phi$
22.5	0	0.2129	0.0011406
45	0	0.2603	0.0025767
67.5	0	0.3312	0.0042842
90	0	0.4149	0.0058086
22.5	2	0.2129	0.0039844
45	2	0.2603	0.0090014
67.5	2	0.3312	0.0149660
90	2	0.4149	0.0202913
22.5	4	0.2129	0.0068283
45	4	0.2603	0.0154260
67.5	4	0.3312	0.0256479
90	4	0.4149	0.0347741
22.5	6	0.2129	0.0096721
45	6	0.2603	0.0218507
67.5	6	0.3312	0.0363297
90	6	0.4149	0.0492568
22.5	8	0.2129	0.0125160
45	8	0.2603	0.0282753
67.5	8	0.3312	0.0470116
90	8	0.4149	0.0637396
22.5	10	0.2129	0.0153598
45	10	0.2603	0.0346999
67.5	10	0.3312	0.0576934
90	10	0.4149	0.0782223

Table 5.8
Values of μ_{ClarkY} & $\mu_{ClarkY}(\alpha - \alpha_{L=0})\sin\phi$ at different AOA

φ (°)	μ	Coefficient of A_1	Coefficient of A_3	Coefficient of A_5	Coefficient of A_7
22.5	0.2129	0.2279	0.9436	1.3370	0.7167
45	0.2603	0.6841	1.0522	-1.4203	-1.7884
67.5	0.3312	1.1596	-0.7338	-0.9873	2.9956
90	0.4149	1.4149	-2.2447	3.0745	-3.9043

Table 5.9 Coefficients of μ_{ClarkY} & A_1, A_3, A_5 , and A_7 values at different φ

$\alpha(^{\circ})$	A_1	A_3	A_5	A_7
0	0.00390	0.00008	0.00014	-0.00001
2	0.01361	0.00028	0.00048	-0.00004
4	0.02333	0.00048	0.00083	-0.00008
6	0.03304	0.00069	0.00118	-0.00011
8	0.04276	0.00089	0.00152	-0.00014
10	0.05248	0.00109	0.00187	-0.0017

Table 5.10 A_1 , A_3 , A_5 , and A_7 at different AOA (Clark Y airfoil)

$\alpha(^{\circ})$	C_L
0	0.0631
2	0.2201
4	0.3773
6	0.5343
8	0.6915
10	0.8487

Table 5.11 C_L values at different AOA (Clark Y airfoil)

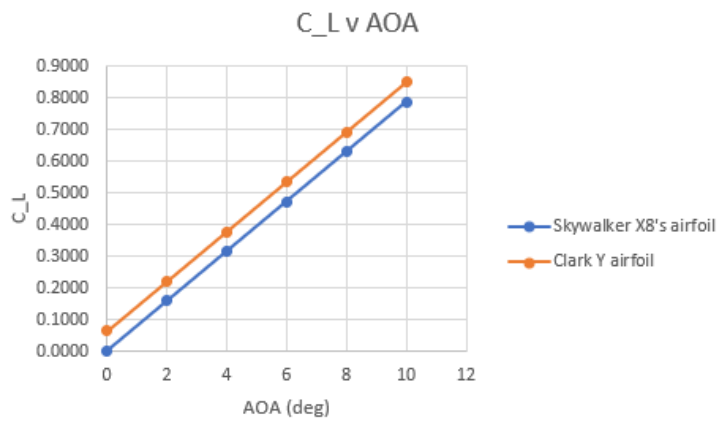
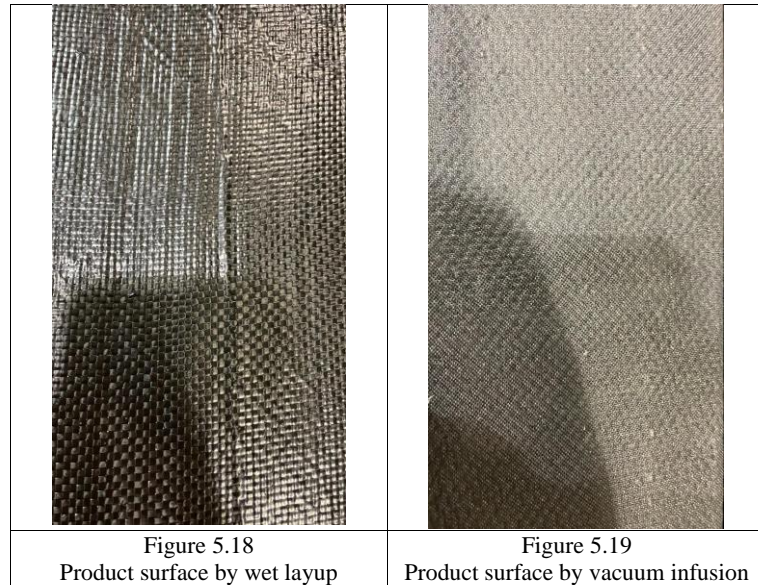


Figure 5.17
 C_L v AOA graph of both airfoils with 382 mm chord length

According to Figure 5.17, the C_L of the Clark Y airfoil was always higher than that of the Skywalker X8's airfoil at different AOA. Hence, by the application of the lifting line theory, it is estimated that the wing of the Clark Y airfoil could have a better aerodynamics performance than that of the Skywalker X8's airfoil.

5.3. Manufacturing of the components of composited wing

5.3.1. *Appearance of components of composited wing*



According to the Figure 5.18 and Figure 5.19, there were some wrinkles on the composited components by the wet layup, while that did not occur during the vacuum infusion. On the other hand, a slippery surface was made by the wet layup, but a rough surface was manufactured by vacuum infusion.



Figure 5.20

Appearance comparison between the products made by wet layup (Left) and vacuum infusion (Right)

By considering the differences in the sequence of the processes and the used equipment between the two manufacturing methods, it was concluded that the slippery surface in wet layup was caused by extra smeared epoxy resin on the surface before vacuuming. For the vacuum infusion, the vacuum film had already compressed the carbon fibre surface before the epoxy resin passed. Therefore, in the condition of high compaction and friction, only less resin could flow on the surface which was not enough to form a slippery resin membrane.

For the difference between wrinkle and flat surfaces, it was because the vacuum pump used in the vacuum infusion was much more powerful which could compact the carbon fibre harder. In addition, the compact flow of resin could also help flatten the carbon fibre. Another explanation was that the condition of the surface of the mold for a wet layup was not as good as the one used for vacuum infusion, which affected the appearance of the final product.

5.3.2. Dimensions of components of composites wing

From Figure 5.21 to Figure 5.25, they showed that the tolerances of the composites parts were small enough as they could fit with each other. The required dimensions of the composites parts could be kept well after the fabrication. Thus, it is believed that after the post-processing and finishing of the parts, they can be used in the next composites manufacturing stage.

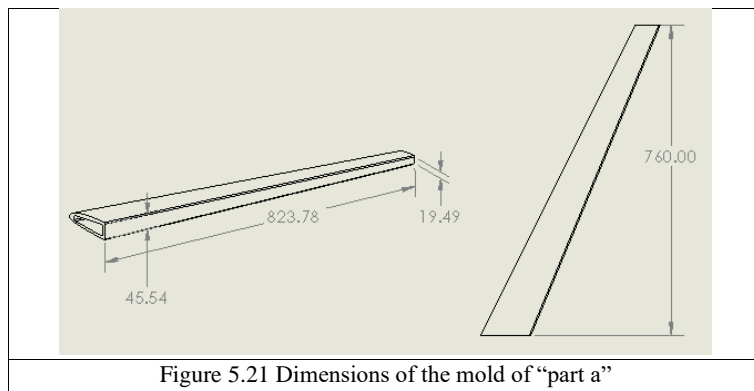


Figure 5.21 Dimensions of the mold of “part a”

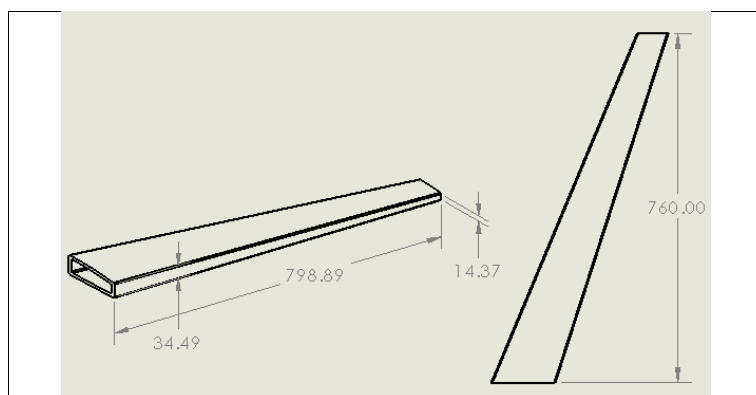


Figure 5.22 Dimensions of the mold of "part b"

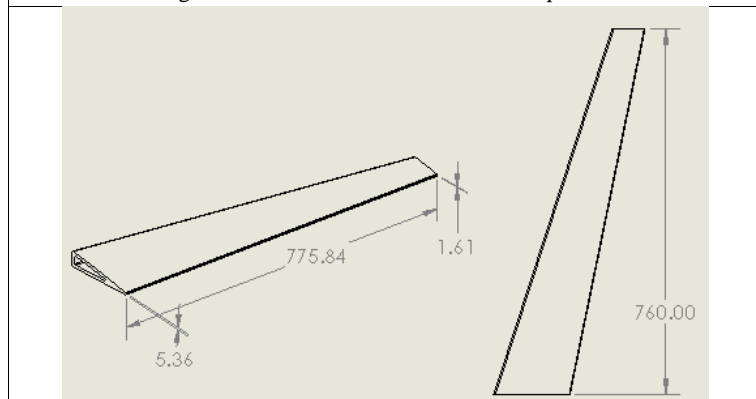


Figure 5.23 Dimensions of the mold of "part c"



Figure 5.24 Top view of the parts (a to c) of the composited wing

5.3.3. Weight of components of composited wing

Components	Weights (g)
Part a	145.2
Part b	165.8
Part c	142.8

Table 5.12 Weights of the three composited components

According to the table above, the weights of the three carbon fiber parts of a wing are around from 140 g to 170 g. Hence, the estimated weight of a composited wing without the transition part should be:

$$W_{CF\ wing\ without\ transition\ part} = (145.2 + 165.8 + 142.8) * 2 = 907.6\ g$$



Figure 5.25 Measuring the weight of part a



Figure 5.26 Measuring the weight of part b



Figure 5.27 Measuring the weight of part c

6. Chapter 6: Recommendations for future work

6.1. Flight test of VTOL Skywalker X8 UAV with payload

Referring to section 5.4, a flight test of the VTOL Skywalker X8 UAV with payload is recommended for further work. Flying the VTOL Skywalker X8 UAV with the same approach as the previous one can clearly identify the relationship between its total weight and its performance. With the result of the flight test, we can compare the flight log we got in the previous flight test.

6.2. 3D CFD simulations of the wings and the whole VTOL UAV

Also from section 5.4, it is recommended that we can do the 3D CFD simulations of the wings and the whole VTOL UAV by using a workstation which is a more powerful computer in the laboratory. Then, we can compare the 3D simulations results with the lifting line theory and the wind tunnel test which is mentioned below.

6.3. Wind tunnel test for the lift and drag forces measurement of the VTOL UAV

We can also put a scaled-down VTOL UAV without all its propellers into a wind tunnel for collecting its c_l and c_d performance at different AOA. The removal of the propellers aims to decrease the effect of the disturbance. A factor (unit: N/V) can be used to multiply the readings of the voltage readings so the readings can be converted into Newton for showing the lift and drag of the VTOL UAV. We can compare the results in this test with the simulation results that we did by CFD.

6.4. Manufacturing two composited wings completely

According to section 5.4, in order to bring about the comprehensive composited manufacturing, we can combine all the six parts of each wing and installed the completed wing next to the fuselage of Skywalker X8 with the full electronic and mechanical components. During the combination process, the six carbon fiber parts will be joined together by laying two more layers of carbon fiber fabric to form a whole wing.

6.5. Flight test of VTOL UAV with composited wings

After the manufacture of the VTOL UAV with composited wings and finishing the assembly of the composited UAV, we can carry out some flight tests to collect and analyze the flight log data using the same approach tried in the Skywalker X8. After that, the results can be compared with the one of the Skywalker X8 and the CFD simulation in order to understand the differences between them.

7. Chapter 7: Conclusion

A new design of the VTOL UAV which was suitable for the mission of air quality monitoring in the Greater Bay Area was developed in this project. The airframe of the VTOL Skywalker X8 UAV and the coordination between the electronic and mechanical components could enable the vehicle to perform distinctively in duration, speed and maneuverability. Especially with the help of the Ansys Fluent simulator, it could be more objective for the judgment of airfoil selection which could make a great improvement on aerodynamics from the original design. Due to the working environment of the UAV, the material replacement was also achieved which brings higher durability than the original foam. For further design implementation, a VTOL Skywalker X8 was built for the reference data that could contribute to the future design. The manufacture of the component of the new design carbon fiber wing was also done by the study of composite material. The project can be further developed by building a whole new composited VTOL UAV with 3D simulation and flight test. This is believed to achieve comprehensive product development from engineering concept to practical application.

References

- [1] (2019). *Trial: Development of vertical take-off and landing (VTOL) unmanned aerial vehicle (UAV) for air quality monitoring in Greater Bay Area.*
- [2] J. Hu and A. Lanzon, "An innovative tri-rotor drone and associated distributed aerial drone swarm control," *Robotics and autonomous systems*, vol. 103, pp. 162-174, 2018, doi: 10.1016/j.robot.2018.02.019.
- [3] L. Cary and J. Coyne, "ICAO Unmanned Aircraft Systems (UAS), Circular 328," *UVS International, Blyenburgh & Co*, vol. 2012, pp. 112-115, 2011.
- [4] I. B. Laskowitz, "Vertical take-off and landing (VTOL) rotorless aircraft with inherent stability," *Annals of the New York Academy of Sciences*, vol. 93, no. 1, pp. 3-24, 1961.
- [5] A. Saini, M. Chhabra, and P. Sujit, "Hybrid VTOL-UAV for air delivery and sampling purposes," 2018.
- [6] G. Dekoulis, C. Yinka-Banjo, and O. Ajayi, "Sky-Farmers: Applications of Unmanned Aerial Vehicles (UAV) in Agriculture," doi: 10.5772/intechopen.89488.
- [7] D. Baek, Y. Chen, A. Bocca, A. Macii, E. Macii, and M. Poncino, "Battery-Aware Energy Model of Drone Delivery Tasks," pp. 1-6, doi: 10.1145/3218603.3218614.
- [8] A. Mathur and E. M. Atkins, "Design, Modeling and Hybrid Control of a QuadPlane," in *AIAA Scitech 2021 Forum*, 2021, p. 0374.
- [9] P. Bhatt and A. Goe, "Carbon fibres: production, properties and potential use," *Material Science Research India*, vol. 14, no. 1, pp. 52-57, 2017.
- [10] S. Kumar Das and S. Roy, "Finite element analysis of aircraft wing using carbon fiber reinforced polymer and glass fiber reinforced polymer," *IOP conference series.*, vol. 402, no. 1, p. 012077, 2018, doi: 10.1088/1757-899X/402/1/012077.
- [11] N. Hashim, D. L. A. Majid, D. M. Baitab, N. Yidris, and R. Zahari, "Tensile Properties of Woven Intra-Ply Carbon/Kevlar Reinforced Epoxy Hybrid Composite at Sub-Ambient Temperature," pp. 766-773, doi: 10.1016/B978-0-12-803581-8.11567-X.
- [12] L. Calabrese, G. Di Bella, and V. Fiore, "Manufacture of marine composite sandwich structures," pp. 57-78, doi: 10.1016/B978-1-78242-250-1.00003-X.
- [13] K. Balasubramanian, M. T. H. Sultan, and N. Rajeswari, "Manufacturing techniques of composites for aerospace applications," pp. 55-67, doi: 10.1016/B978-0-08-102131-6.00004-9.
- [14] R. A. Shenoi and A. R. Dodkins, "Design of Ships and Marine Structures Made from FRP Composite Materials," pp. 429-449, doi: 10.1016/B0-08-042993-9/00117-0.
- [15] Skywalker X8. <http://skywalkermodel.com/en/76.html> (accessed 20 Nov, 2021).
- [16] T. International Conference on Unmanned Aircraft Systems Dallas, "Aerodynamic modeling of the Skywalker X8 Fixed-Wing Unmanned Aerial Vehicle," pp. 826-835, 2018, doi: 10.1109/ICUAS.2018.8453370.
- [17] "CLARK Y AIRFOIL (clarky-il)." Airfoil Tool. <http://airfoiltools.com/airfoil/details?airfoil=clarky-il#polars> (accessed 20 Nov, 2021).
- [18] Cadence, "Compute Grid Spacing for a Given Y+." [Online]. Available: <https://www.pointwise.com/yplus/index.html>
- [19] "Infusion." Sicomin Epoxy Systems. <http://sicomin.com/products/vacuum-and-infusion/infusion> (accessed 22 Mar, 2022).

- [20] A. Tools, "CLARK Y AIRFOIL (clarky-il) Xfoil prediction polar at RE=1,000,000 Ncrit=9." [Online]. Available: <http://airfoiltools.com/polar/details?polar=xf-clarky-il-1000000>

Appendix I: Video of indoor hovering test



QR code of the video of VTOL Skywalker X8's indoor hovering test

(Link: https://youtu.be/cd0E_a2m0yM)

Appendix II: Video of flight test without payload



QR code of the video of VTOL Skywalker X8's flight test without payload

(Link: <https://youtu.be/xZHm2rkBqb8>)

Appendix III: Video of vacuum infusion for manufacturing composites wing



QR code of the video of vacuum infusion for manufacturing composites wing

(Link: <https://youtu.be/1HfRb3bHXTc>)

Appendix IV: Coordinates of Clark Y airfoil (chord length = 1 m)

	1	0	0	0		1	1	0	0	0	
1	2	0.0005	0.002339	0		1	2	0.0005	-0.00467	0	
1	3	0.001	0.0037271	0		1	3	0.001	-0.0059418	0	
1	4	0.002	0.0058025	0		1	4	0.002	-0.0078113	0	
1	5	0.004	0.0089238	0		1	5	0.004	-0.0105126	0	
1	6	0.008	0.013735	0		1	6	0.008	-0.0142862	0	
1	7	0.012	0.0178581	0		1	7	0.012	-0.0169733	0	
1	8	0.02	0.0253735	0		1	8	0.02	-0.0202723	0	
1	9	0.03	0.0330215	0		1	9	0.03	-0.0226056	0	
1	10	0.04	0.0391283	0		1	10	0.04	-0.0245211	0	
1	11	0.05	0.0442753	0		1	11	0.05	-0.0260452	0	
1	12	0.06	0.0487571	0		1	12	0.06	-0.0271277	0	
1	13	0.08	0.0564308	0		1	13	0.08	-0.0284595	0	
1	14	0.1	0.0629981	0		1	14	0.1	-0.0293786	0	
1	15	0.12	0.0686204	0		1	15	0.12	-0.0299633	0	
1	16	0.14	0.0734346	0		1	16	0.14	-0.0302404	0	
1	17	0.16	0.0775707	0		1	17	0.16	-0.0302546	0	
1	18	0.18	0.0810687	0		1	18	0.18	-0.030049	0	
1	19	0.2	0.0839202	0		1	19	0.2	-0.0296656	0	
1	20	0.22	0.0861433	0		1	20	0.22	-0.0291445	0	
1	21	0.24	0.0878308	0		1	21	0.24	-0.0285181	0	
1	22	0.26	0.089084	0		1	22	0.26	-0.0278164	0	
1	23	0.28	0.0900016	0		1	23	0.28	-0.0270696	0	
1	24	0.3	0.0906804	0		1	24	0.3	-0.0263079	0	
1	25	0.32	0.0911857	0		1	25	0.32	-0.0255565	0	
1	26	0.34	0.0915079	0		1	26	0.34	-0.0248176	0	
1	27	0.36	0.0916266	0		1	27	0.36	-0.024087	0	
1	28	0.38	0.0915212	0		1	28	0.38	-0.0233606	0	
1	29	0.4	0.0911712	0		1	29	0.4	-0.0226341	0	
1	30	0.42	0.0905657	0		1	30	0.42	-0.0219042	0	
1	31	0.44	0.0897175	0		1	31	0.44	-0.0211708	0	
1	32	0.46	0.0886427	0		1	32	0.46	-0.0204353	0	
1	33	0.48	0.0873572	0		1	33	0.48	-0.0196986	0	
1	34	0.5	0.0858772	0		1	34	0.5	-0.0189619	0	
1	35	0.52	0.0842145	0		1	35	0.52	-0.0182626	0	
1	36	0.54	0.0823712	0		1	36	0.54	-0.0174914	0	
1	37	0.56	0.080348	0		1	37	0.56	-0.0167572	0	
1	38	0.58	0.0781451	0		1	38	0.58	-0.0160232	0	
1	39	0.6	0.0757633	0		1	39	0.6	-0.0152893	0	
1	40	0.62	0.0732055	0		1	40	0.62	-0.0145551	0	
1	41	0.64	0.0704822	0		1	41	0.64	-0.0138207	0	
1	42	0.66	0.0676046	0		1	42	0.66	-0.0130862	0	
1	43	0.68	0.0645843	0		1	43	0.68	-0.0123515	0	
1	44	0.7	0.0614329	0		1	44	0.7	-0.0116169	0	
1	45	0.72	0.0581599	0		1	45	0.72	-0.0108823	0	
1	46	0.74	0.0547675	0		1	46	0.74	-0.0101478	0	
1	47	0.76	0.0512565	0		1	47	0.76	-0.0094133	0	
1	48	0.78	0.0476281	0		1	48	0.78	-0.0086788	0	
1	49	0.8	0.0438836	0		1	49	0.8	-0.0079443	0	
1	50	0.82	0.0400245	0		1	50	0.82	-0.0072098	0	
1	51	0.84	0.0360536	0		1	51	0.84	-0.0064753	0	
1	52	0.86	0.031974	0		1	52	0.86	-0.0057408	0	
1	53	0.88	0.0277891	0		1	53	0.88	-0.0050063	0	
1	54	0.9	0.0235025	0		1	54	0.9	-0.0042718	0	
1	55	0.92	0.0191156	0		1	55	0.92	-0.0035373	0	
1	56	0.94	0.0146239	0		1	56	0.94	-0.0028028	0	
1	57	0.96	0.0100232	0		1	57	0.96	-0.0020683	0	
1	58	0.97	0.0076868	0		1	58	0.97	-0.0017011	0	
1	59	0.98	0.0053335	0		1	59	0.98	-0.0013339	0	
1	60	0.99	0.002969	0		1	60	0.99	-0.0009666	0	
1	61	1	0	0		1	61	1	0	0	

Appendix V: Coordinates of Clark Y airfoil (chord length = 382 mm)

1	1	0	0	0		1	1	0.382	0	0
1	2	0.000191	0.000893498	0		1	2	0.37818	-0.000369241	0
1	3	0.000382	0.001423752	0		1	3	0.37436	-0.00050955	0
1	4	0.000764	0.002216555	0		1	4	0.37054	-0.00064982	0
1	5	0.001528	0.003408892	0		1	5	0.36672	-0.000790091	0
1	6	0.003056	0.00524677	0		1	6	0.35908	-0.00107067	0
1	7	0.004584	0.006821794	0		1	7	0.35144	-0.001351249	0
1	8	0.00764	0.009692677	0		1	8	0.3438	-0.001631828	0
1	9	0.01146	0.012614213	0		1	9	0.33616	-0.001912407	0
1	10	0.01528	0.014947011	0		1	10	0.32852	-0.002192986	0
1	11	0.0191	0.016913165	0		1	11	0.32088	-0.002473565	0
1	12	0.02292	0.018625212	0		1	12	0.31324	-0.002754144	0
1	13	0.03056	0.021556566	0		1	13	0.3056	-0.003034723	0
1	14	0.0382	0.024065274	0		1	14	0.29796	-0.003315302	0
1	15	0.04584	0.026212993	0		1	15	0.29032	-0.003595881	0
1	16	0.05348	0.028052552	0		1	16	0.28268	-0.00387646	0
1	17	0.06112	0.029632007	0		1	17	0.27504	-0.004157039	0
1	18	0.06876	0.030968243	0		1	18	0.2674	-0.004437656	0
1	19	0.0764	0.032057516	0		1	19	0.25976	-0.004718273	0
1	20	0.08404	0.032906741	0		1	20	0.25212	-0.004998928	0
1	21	0.09168	0.033551366	0		1	21	0.24448	-0.005279507	0
1	22	0.09932	0.034030088	0		1	22	0.23684	-0.005560048	0
1	23	0.10696	0.034388611	0		1	23	0.2292	-0.005840513	0
1	24	0.1146	0.034639913	0		1	24	0.22156	-0.006120862	0
1	25	0.12224	0.034832937	0		1	25	0.21392	-0.00640125	0
1	26	0.12988	0.034956018	0		1	26	0.20628	-0.006681715	0
1	27	0.13752	0.035001361	0		1	27	0.19864	-0.006962408	0
1	28	0.14516	0.034961098	0		1	28	0.191	-0.007243446	0
1	29	0.1528	0.034827398	0		1	29	0.18336	-0.007524865	0
1	30	0.16044	0.034596097	0		1	30	0.17572	-0.007806285	0
1	31	0.16808	0.034272085	0		1	31	0.16888	-0.008087246	0
1	32	0.17572	0.033861511	0		1	32	0.16044	-0.008367404	0
1	33	0.18336	0.03337045	0		1	33	0.1528	-0.008646226	0
1	34	0.191	0.03280509	0		1	34	0.14516	-0.008923749	0
1	35	0.19864	0.032169939	0		1	35	0.13752	-0.009201234	0
1	36	0.20628	0.031465798	0		1	36	0.12988	-0.009480323	0
1	37	0.21392	0.030692936	0		1	37	0.12224	-0.009762583	0
1	38	0.22156	0.029851428	0		1	38	0.1146	-0.010049618	0
1	39	0.2292	0.028941581	0		1	39	0.10696	-0.010340587	0
1	40	0.23684	0.027964501	0		1	40	0.09932	-0.010625865	0
1	41	0.24448	0.0269242	0		1	41	0.09168	-0.010893914	0
1	42	0.25212	0.025824957	0		1	42	0.08484	-0.011133199	0
1	43	0.25976	0.024671203	0		1	43	0.0764	-0.011332259	0
1	44	0.2674	0.023467368	0		1	44	0.06876	-0.011478718	0
1	45	0.27504	0.022217082	0		1	45	0.06112	-0.011557257	0
1	46	0.28268	0.020921185	0		1	46	0.05348	-0.011551833	0
1	47	0.29032	0.019579983	0		1	47	0.04584	-0.011445981	0
1	48	0.29796	0.018193934	0		1	48	0.0382	-0.01222625	0
1	49	0.3056	0.016763535	0		1	49	0.03056	-0.010871529	0
1	50	0.31324	0.015289359	0		1	50	0.02292	-0.010362781	0
1	51	0.32088	0.013772475	0		1	51	0.0191	-0.009949266	0
1	52	0.32852	0.012214068	0		1	52	0.01528	-0.00936706	0
1	53	0.33616	0.010615436	0		1	53	0.01146	-0.008635339	0
1	54	0.3438	0.008977955	0		1	54	0.00764	-0.007744019	0
1	55	0.35144	0.007302159	0		1	55	0.004584	-0.006483801	0
1	56	0.35908	0.00558633	0		1	56	0.003056	-0.005457328	0
1	57	0.36672	0.003828862	0		1	57	0.001528	-0.004015813	0
1	58	0.37054	0.002936358	0		1	58	0.000764	-0.002983917	0
1	59	0.37436	0.002037397	0		1	59	0.000382	-0.002269768	0
1	60	0.37818	0.001134158	0		1	60	0.000191	-0.00178394	0
1	61	0.382	0	0		1	61	0	0	0

Coordinates of its upper surface Coordinates of its lower surface

Appendix VI: Coordinates of Skywalker X8's airfoil (chord length = 382 mm)

	1	0	0	0		1	1	0	0	0
1	2	0.001518569	0.004215564	0	1	2	0.00146858	-0.003360219	0	
1	3	0.005622838	0.007864378	0	1	3	0.004545419	-0.005843502	0	
1	4	0.018413302	0.010589538	0	1	4	0.008463595	-0.007524409	0	
1	5	0.017119786	0.013418452	0	1	5	0.012895936	-0.008544804	0	
1	6	0.021586514	0.019496567	0	1	6	0.017119786	-0.008976844	0	
1	7	0.027333537	0.016634565	0	1	7	0.021174015	-0.0091216405	0	
1	8	0.031441408	0.017692521	0	1	8	0.026919509	-0.009474502	0	
1	9	0.039326273	0.019494921	0	1	9	0.031214187	-0.009681423	0	
1	10	0.046110553	0.020846299	0	1	10	0.035076042	-0.009858572	0	
1	11	0.053899149	0.02174471	0	1	11	0.041205009	-0.010129151	0	
1	12	0.059872812	0.022927436	0	1	12	0.046871619	-0.010365562	0	
1	13	0.064911715	0.02365602	0	1	13	0.052830468	-0.010599998	0	
1	14	0.072318019	0.024399994	0	1	14	0.0593083707	-0.010837924	0	
1	15	0.077826329	0.024826498	0	1	15	0.066046271	-0.011067503	0	
1	16	0.083670957	0.025164713	0	1	16	0.07142368	-0.011237186	0	
1	17	0.091462434	0.025439593	0	1	17	0.077629571	-0.011418219	0	
1	18	0.098619998	0.025523224	0	1	18	0.084622479	-0.011608321	0	
1	19	0.1054758	0.025460134	0	1	19	0.090299985	-0.011738401	0	
1	20	0.11292999	0.025424236	0	1	20	0.094345163	-0.011826976	0	
1	21	0.118770516	0.024970266	0	1	21	0.101089941	-0.011959328	0	
1	22	0.124313157	0.024635242	0	1	22	0.10781495	-0.012072681	0	
1	23	0.131906345	0.02406358	0	1	23	0.114306462	-0.012164423	0	
1	24	0.137527145	0.0235363703	0	1	24	0.120747103	-0.012238394	0	
1	25	0.14305598	0.023014087	0	1	25	0.128519559	-0.012384723	0	
1	26	0.148623552	0.022407838	0	1	26	0.138223752	-0.012352741	0	
1	27	0.15450695	0.021715604	0	1	27	0.148464433	-0.012361369	0	
1	28	0.161075335	0.020887319	0	1	28	0.159240887	-0.012323824	0	
1	29	0.166513094	0.020163565	0	1	29	0.168880645	-0.012249723	0	
1	30	0.17190477	0.019416962	0	1	30	0.176969405	-0.012161559	0	
1	31	0.178024193	0.018548556	0	1	31	0.185834243	-0.012026567	0	
1	32	0.185905601	0.01737675	0	1	32	0.192560245	-0.011905254	0	
1	33	0.194282017	0.016111005	0	1	33	0.200100394	-0.011747096	0	
1	34	0.200826957	0.015111488	0	1	34	0.208421202	-0.011545386	0	
1	35	0.2064168	0.01425661	0	1	35	0.21647411	-0.011323016	0	
1	36	0.210992623	0.013559291	0	1	36	0.222657972	-0.011134125	0	
1	37	0.216205444	0.012770606	0	1	37	0.229915192	-0.010892534	0	
1	38	0.220991293	0.01206811	0	1	38	0.2362682194	-0.010649402	0	
1	39	0.226378066	0.0121261455	0	1	39	0.244675461	-0.01033369	0	
1	40	0.231017436	0.010591274	0	1	40	0.252724168	-0.009991232	0	
1	41	0.234626674	0.010130234	0	1	41	0.261579777	-0.009583601	0	
1	42	0.240113121	0.0099317891	0	1	42	0.27043871	-0.009143482	0	
1	43	0.246750278	0.008435564	0	1	43	0.277149821	-0.008788536	0	
1	44	0.253980809	0.007528283	0	1	44	0.284659552	-0.008369343	0	
1	45	0.259469462	0.0068680402	0	1	45	0.291631968	-0.007959333	0	
1	46	0.265727885	0.0061151255	0	1	46	0.298383245	-0.007546064	0	
1	47	0.271391569	0.005550824	0	1	47	0.304504025	-0.007149729	0	
1	48	0.276270447	0.00506635	0	1	48	0.311206695	-0.006701132	0	
1	49	0.282405143	0.004498434	0	1	49	0.316840884	-0.00630976	0	
1	50	0.290494049	0.003815726	0	1	50	0.322462706	-0.005906087	0	
1	51	0.296233169	0.003374746	0	1	51	0.328367395	-0.005468129	0	
1	52	0.30076785	0.003050978	0	1	52	0.33346696	-0.00507878	0	
1	53	0.307577921	0.002604951	0	1	53	0.339885841	-0.004572404	0	
1	54	0.314396749	0.00220648	0	1	54	0.344965442	-0.004160003	0	
1	55	0.320603917	0.00188611	0	1	55	0.350055389	-0.003736085	0	
1	56	0.326162621	0.001634473	0	1	56	0.354464645	-0.00360219	0	
1	57	0.330420519	0.001465192	0	1	57	0.357751516	-0.003063087	0	
1	58	0.333911845	0.001342301	0	1	58	0.360459072	-0.002797265	0	
1	59	0.337307755	0.001247507	0	1	59	0.363709517	-0.002452997	0	
1	60	0.342283836	0.001093125	0	1	60	0.366957584	-0.002081471	0	
1	61	0.346742316	0.000984149	0	1	61	0.368817103	-0.00185636	0	
1	62	0.350696081	0.000873783	0	1	62	0.370442366	-0.00165219	0	
1	63	0.354464696	0.000768585	0	1	63	0.37161777	-0.001500215	0	
1	64	0.356638798	0.000707897	0	1	64	0.372944135	-0.001324363	0	
1	65	0.359564077	0.00062624	0	1	65	0.374471202	-0.001116171	0	
1	66	0.362016263	0.000557789	0	1	66	0.375837507	-0.000924691	0	
1	67	0.364964017	0.000475505	0	1	67	0.377262362	-0.00071976	0	
1	68	0.367544072	0.000404585	0	1	68	0.378153914	-0.000588005	0	
1	69	0.371588359	0.000296952	0	1	69	0.379235129	-0.000247173	0	
1	70	0.374225885	0.000216968	0	1	70	0.380263412	-0.000270583	0	
1	71	0.378001706	0.000111569	0	1	71	0.381198801	-0.000125707	0	
1	72	0.381998548	0	0	1	72	0.381998548	0	0	

Appendix VII: List of Figures

Chapter 1

Figure 1.1 Our VTOL Skywalker X8 UAV	13
Figure 1.2 Dummy air quality sensor.....	13

Chapter 2

Figure2.1 UAV weight and payload vs. flight time.	20
Figure2.2 Forces on quadcopter in VTOL mode (a) and thrust mode (b).....	20
Figure2.3 A “4+1” fixed-wing VTOL UAV which was built by one of our teammates.....	23
Figure2.4 A VTOL aircraft with its four motors (M_1, M_2, M_3 and M_4).....	23
Figure2.5 Wing deformation under pressure.....	27
Figure2.6 Maximum amplitude(mm) of vibration of different materials and wing mode shapes	27
Figure2.7 Working principle of vacuum infusion.....	28
Figure2.8 Wet hand layup method	30
Figure2.9 Wet layup method with vacuum assisted molding.....	30

Chapter 3

Figure3.1 & 3.2 Gantt chart of actual progress under pandemic.....	32
Figure3.3 Flight test of Skywalker X8 without payload in Yuen Long	33
Figure3.4 Simulation of Clark Y airfoil by Ansys Fluent	34
Figure3.5 Composite wing parts manufactured in this project (without mold release)	35
Figure3.6 3D X8 model in Ansys Fluent	36
Figure3.7 cl graph of the 3D Skywalker X8	37

Chapter 4

Figure4.1 Design flowchart of building a VTOL UAV	39
Figure4.2 Design flowchart of manufacturing of composited wings	40
Figure4.3 Design flowchart of vacuum infusion	41
Figure4.4 Design flowchart of wet layup with vacuum bagging	42

Figure4.5 Structure of Skywalker X8.....	43
Figure4.6 Motor-propeller performance analysis.....	45
Figure4.7 Overview of the VTOL part of our VTOL Skywalker X8 UAV	47
Figure4.8 Electronics wires are inserted into the carbon fiber tubes	47
Figure4.9 Connection of the VTOL Skywalker X8 UAV's electronics components	48
Figure4.10 Electronic wires management inside a wing.....	49
Figure4.11 Power Management board in VTOL Skywalker X8 UAV	49
Figure4.12 Indoor hovering test of VTOL Skywalker X8	50
Figure4.13 Using handySCAN to do the 3D scanning	51
Figure4.14 Progress while aligning the wing	52
Figure4.15 Results after aligning the wing	52
Figure4.16 Results after aligning the fuselage	53
Figure4.17 Results after aligning the wing	53
Figure4.18 Convening the cross-section into entities	54
Figure4.19 – 4.24 3D scanned curves and their CAD drawing.....	55
Figure4.25 Lift coefficient vs. drag coefficient of Skywalker X8[16].....	56
Figure4.26 Lift coefficient vs. angle-of-attack of Skywalker X8[16].....	56
Figure4.27 Lift coefficient vs. drag coefficient of Clark Y airfoil[17]	56
Figure4.28 Lift coefficient vs. angle-of-attack of Clark Y airfoil[17]	56
Figure4.29 Shape of Clark Y airfoil[17]	56
Figure4.30 Shape of the airfoil of Skywalker X8	57
Figure4.31 Imported Clark Y airfoil with chord length = 1 m.....	58
Figure4.32 Drawing Wind tunnel for the airfoils' simulation.....	60
Figure4.33 Spalart-Allmaras Model in Ansys Fluent.....	61
Figure4.34 $u +$ vs $y +$ graph	62
Figure4.35 Calculation of the wall spacing referring to $y+ = 1$ &	63
Figure4.36 edges around the chord	63
Figure4.37 Calculation of the length of the first element.....	64

Figure4.38 $y +$ of the Clark Y airfoil with 1 m chord length at 0 deg of AOA....	64
Figure4.39 $y +$ of the Skywalker X8's airfoil with 382 mm chord length at 0 deg of AOA.....	65
Figure4.40 $y +$ of the Clark Y airfoil with 382 mm chord length at 0 deg of AOA	65
Figure4.41 Inlet velocity setting in Ansys Fluent	66
Figure4.42 & 4.43 Boundary conditions of Clark Y airfoil with 1 m chord length at 2 deg of AOA with number of divisions = 200.....	67
Figure4.44 & 4.45 Boundary conditions of Clark Y airfoil with 382 mm chord length at 4 deg of AOA with number of divisions = 200.....	68
Figure4.46 & 4.47 Boundary conditions of Clark Y airfoil with 382 mm chord length at 4 deg of AOA with number of divisions = 200.....	69
Figure4.48 x-component and the y-component of the force vector for the lift and drag report definition and the inlet velocity (AOA in radians).....	70
Figure4.49 Lift report definition when AOA = 0 degree	71
Figure4.50 Capture of the converged results of the Clark Y airfoil (1 m chord length) at 0 deg of AOA	72
Figure4.51 Mesh of Clark Y airfoil (1m chord length) when no. of division = 200	73
Figure4.52 Mesh of Clark Y airfoil (1m chord length) when no. of division = 250	73
Figure4.53 Meshh of Clark Y airfoil (1m chord length) when no. of division = 200 (close-up).....	73
Figure4.54 Mesh of Clark Y airfoil (1m chord length) when no. of division = 250(close-up).....	73
Figure4.55 Results of the Clark Y airfoil (1m chord length) when no. of division of its mesh = 200.....	74
Figure4.56 Results of the Clark Y airfoil (1m chord length) when no. of division of its mesh = 250.....	74
Figure4.57 Dimensions of a composited wing	76
Figure4.58 CAD drawing of a composited wing	76
Figure4.59 Dimensions of a Skywalker X8's wing (without connection with winglet)	76

Figure4.60 CAD drawing of a Skywalker X8's wing (without connection with winglet)	76
Figure4.61 VTOL UAV with composited wings (made of carbon fibre)	77
Figure4.62 VTOL UAV with original wings (made of polystyrene)	77
Figure4.63 "Part a" of the right composited wing.....	79
Figure4.64 "Part b" of the right composited wing	79
Figure4.65 "Part c" of the right composited wing.....	79
Figure4.66 "Part di" of the right composited wing	79
Figure4.67 "Part dii" of te right composited wing	79
Figure4.68 "Part diii" of the right composited wing	79
Figure4.69 Combination of 6 molds of a composited wing	79
Figure4.70 CAD drawing of the connection part between the wing and the winglet	80
Figure4.71 Assembly of connection of the wing and the winglet	80
Figure4.72 Cross section of the carbon fiber mold layers[19]	81
Figure4.73 Lay up of carbon fiber fabric, where seam located in the bonding surfaces.....	82
Figure4.74 Setup of vacuum infusion	83
Figure4.75 Infusion of epoxy resin	84
Figure4.76 Completion of infusion	85
Figure4.77 Layup of the CF mold	86
Figure4.78 Wet layup method with vacuum assisted molding.....	87
Figure4.79 CF wing parts released from the molds	88

Chapter 5

Figure5.1 Altitude graph of the flight test	89
Figure5.2 The voltage and current graph of the flight test	90
Figure5.3 Speed graph of the flight test	91
Figure5.4 Residuals graph of the Clark Y airfoil with 1 m chord length at 8 deg of AOA	92
Figure5.5 <i>cl</i> graph of the Clark Y airfoil with 1 m chord length at 8 deg of AOA	93

Figure5.6 cd graph of the Clark Y airfoil with 1 m chord length at 8 deg of AOA	93
Figure5.7 c_l vs AOA graph of the Clark Y airfoil (1 m chord length) by simulations	94
Figure5.8 Standard cl vs AOA graph of the Clark Y airfoil (1 m chord length) when $Re = 1000000$ [20].....	94
Figure5.9 cd vs AOA graph of the Clark Y airfoil (1 m chord length) by simulations	95
Figure5.10 Standard c_d vs AOA graph of the Clark Y airfoil (1 m chord length) when $Re = 1000000$	95
Figure5.11 c_l vs AOA graph of the Skywalker X8's airfoil (382 mm chord length)	97
Figure5.12 cl vs AOA graph of the Clark Y airfoil (382 mm chord length)	97
Figure5.13 c_d vs AOA graph of the Skywalker X8's airfoil (382 mm chord length)	97
Figure5.14 cd vs AOA graph of the Clark Y airfoil (382 mm chord length)	98
Figure5.15 c_l/c_d vs AOA graph of Skywalker X8's airfoil and Clark Y airfoil (chord lengths = 382 mm)	98
Figure5.16 C_l v AOA graph of the Skywalker X8's airfoil with 382 mm chord length.	105
Figure5.17 C_l v AOA graph of both airfoils wih 382 mm chord length.....	107
Figure5.18 Product surface by wet layup	108
Figure5.19 Product surface by vacuum infusion.....	108
Figure5.20 Appearance comparison between the products made by wet layup (Left) and vacuum infusion (Right)	109
Figure5.21 Dimensions of the mold of "part a"	110
Figure5.22 Dimensions of the mold of "part b"	111
Figure5.23 Dimensions of the mold of "part c"	111
Figure5.24 Top view of the parts (a to c) of the composited wing	112
Figure5.25 Measuring the weight of part a	113
Figure5.26 Measuring the weight of part b	113
Figure5.27 Measuring the weight of part c	113

Appendix VIII: List of Tables

Chapter 2

Table 2.1 Comparison of the UAVs	22
Table 2.2 Young modulus and densities of IM Carbon Fiber, Steel and Polystyrene.....	27

Chapter 3

Table 3.1 Original project schedule	31
---	----

Chapter 4

Table 4.1 Specification of Skywalker X8[15].....	43
Table 4.2 Take-off Weight Estimation before VTOL motors selection.....	44
Table 4.3 Comparison of different motor-propeller combinations	46
Table 4.4 Accessories of the VTOL Skywalker X8	46
Table 4.5 Mesh size of the airfoils	60

Chapter 5

Table 5.1 Simulation results of Skywalker X8's airfoil with 382 mm chord length	96
Table 5.2 Simulation results of Clark Y airfoil with 382 mm chord length.....	96
Table 5.3 Required parameters for calculating the CL by lifting line theory	100
Table 5.4 Values of $\mu_{SkywalkerX8}$ & $\mu_{SkywalkerX8}(\alpha - \alpha_{L=0})\sin\phi$ at different AOA	103
Table 5.5 Coefficients of $\mu_{SkywalkerX8}$ & A_1, A_3, A_5 , and A_7 values at different φ	104
Table 5.6 A_1, A_3, A_5 , and A_7 at different AOA (Skywalker X8's airfoil)	104
Table 5.7 CL values at different AOA (Skywalker X8's airfoil)	104
Table 5.8 Values of μ_{ClarkY} & $\mu_{ClarkY}(\alpha - \alpha_{L=0})\sin\phi$ at different AOA.....	106
Table 5.9 Coefficients of μ_{ClarkY} & A_1, A_3, A_5 , and A_7 values at different φ	106
Table 5.10 A_1, A_3, A_5 , and A_7 at different AOA (Clark Y airfoil).....	107
Table 5.11 CL values at different AOA (Clark Y airfoil).....	107
Table 5.12 Weight of the components measured	Error! Bookmark not defined. 112

